THE CONTRIBUTION OF PROTEORHODOPSIN TO THE CELLULAR ENERGY BUDGET OF THE ANTARCTIC DIATOM *PSEUDO-NITZSCHIA SUBCURVATA*

by

KAYLIE HOPE PLUMB

(Under the Direction of Brian M. Hopkinson)

ABSTRACT

Proteorhodopsin (PR) is a proton-pumping protein powered by light that can be used to generate energy, potentially powering ATP synthase. Transcripts for a PR-like gene have been isolated in some species of temperate and polar diatoms. A study investigating the distribution of the PR-like genes showed that they are mostly found in regions of the ocean that experience iron limitation. This suggests that the diatoms may use PR as a supplement to conventional photosynthesis during iron limitation. The following project uses physiological measurements and mass spectrometry-based quantitative proteomics to examine energy flow through the conventional photosynthetic system and compare it to energy flow through PR under varying levels of iron limitation. One PR containing diatom was studied alongside two non-PR containing diatoms for comparison. There was insufficient evidence to conclude that PR provided enough supplemental energy to increase the cellular energy budget of the PR containing diatom under iron limitation.

INDEX WORDS: Diatoms, Southern Ocean, Iron Limitation, Photosynthesis, Proteorhodopsin, Proteomics

THE CONTRIBUTION OF PROTEORHODOPSIN TO THE CELLULAR ENERGY BUDGET OF THE ANTARCTIC DIATOM *PSEUDO-NITZSCHIA SUBCURVATA*

by

KAYLIE HOPE PLUMB

B.S., UNIVERSITY OF SOUTH CAROLINA, 2018

A Thesis Submitted to the Graduate Faculty of The University of Georgia in Partial Fulfillment of the Requirements for the Degree

MASTER OF SCIENCE

ATHENS, GEORGIA

2021

THE CONTRIBUTION OF PROTEORHODOPSIN TO THE CELLULAR ENERGY BUDGET OF THE ANTARCTIC DIATOM *PSEUDO-NITZSCHIA SUBCURVATA*

by

KAYLIE HOPE PLUMB

Major Professor:	Brian Hopkinson
Committee:	Mary Ann Moran
	Adrian Burd

Electronic Version Approved:

Ron Walcott
Dean of the Graduate School
The University of Georgia
August 2021

DEDICATION

I dedicate this thesis to my family who has always supported and nurtured my interest in science. I especially dedicate this work to my grandmother, Karen Plumb, who passed away this year. Her memory reminds me of the gratitude I feel to be surrounded by those who encourage and believe in me.

ACKNOWLEDGEMENTS

I would like to thank my advisor, Dr. Brian Hopkinson, for all his help and guidance during my time at UGA. I also thank my committee members Dr. Mary Ann Moran and Dr. Adrian Burd for encouraging me to grow as a scientist. I would also like to thank Dr. Adrian Marchetti for hosting me in his laboratory at the University of North Carolina – Chapel Hill and Dr. Sarah Andrews for the immense time commitment and effort she put into culturing the diatoms for this experiment. Thanks to Gwendolyn Gallagher in the Waldbauer lab at the University of Chicago for recommending a protein extraction procedure and to Dr. Chau-wen Chou at the University of Georgia Proteomics and Mass Spectrometry Facility for operation of the mass spectrometer (funded by NIH grant 1S10RR02885) detailed in this project. I also acknowledge and thank the National Science Foundation (OPP 1744760) for funding this work.

TABLE OF CONTENTS

Page

INTRODUCTION

Phytoplankton, unicellular autotrophs found throughout the world's oceans, have a powerful impact on the biogeochemistry of the both the atmosphere and oceans (Sarmiento & Bender, 1994). It is well established that phytoplankton are important in sequestering CO_2 from the atmosphere and are a substantial source of O_2 (Falkowski, 1994). Due to our changing climate, it is becoming more important to understand how environmental conditions may limit or change the growth and metabolism of phytoplankton and, by extension, further impact the global climate (Moore et al., 2000; Watson et al., 2000).

Phytoplankton in the Southern Ocean are thought to play a disproportionate role in influencing global climate patterns in comparison to other, larger water masses (Sarmiento et al., 1998). The Southern Ocean has some of the highest stocks of macronutrients in the world yet contains an unexpectedly low phytoplankton biomass considering the availability of nutrients (Levitus et al., 1993). This discrepancy between macronutrient and chlorophyll concentrations classify the Southern Ocean as a high nutrient, low chlorophyll zone (HNLC) (Boyd et al., 2007). Lack of iron supply to the surface waters of the Southern Ocean is the main limiting factor causing low phytoplankton biomass, as has been illustrated by the rapid growth of phytoplankton after addition of iron to patches of Southern Ocean waters (Martin, 1990; Edwards & Sedwick, 2001; Boyd et al., 2007; Strzepek et al., 2011). However, in addition to low iron availability, the Southern Ocean undergoes strong changes in light availability due to seasonal forcing as well as sea-ice cover (Kennedy et al., 2019). Light can be a more important limiting factor than iron for communities associated with sea-ice in the Southern Ocean (Peters

& Thomas, 1996; Arrigo, 2014). Phytoplankton indigenous to the Southern Ocean must therefore overcome both iron and light limitation in order to persist (W. G. Sunda & Huntsman, 1997; Boyd et al., 1999; Boyd, 2002; Strzepek et al., 2011).

Diatoms, a group of eukaryotic phytoplankton, are one of the most important taxa of phytoplankton, accounting for ~40% of global oceanic primary production (Luo et al., 2014). They have been the subject of many studies focused on elucidating the numerous adaptations contained in their genome, transcriptome, and proteome that may explain their worldwide dominance in many phytoplankton communities, especially in highly productive regions (Lommer et al., 2012; Nunn et al., 2013; Muhseen et al., 2015; Cohen et al., 2018; Kennedy et al., 2019). Though diatoms are typically confined to more productive regions in tropical and temperate waters, the lack of cyanobacterial competitors in polar regions expands their niche, making diatoms extremely successful in harsh polar environments such as the Southern Ocean (Arrigo et al., 1999; Boyd et al., 2007).

Part of diatoms' success in highly productive waters is their ability to rapidly respond to transient nutrient input events. For example, diatoms have often responded more rapidly and efficiently to iron fertilization experiments when compared to other components of the local community, with the end result being a community dominated by diatoms (de Baar et al., 2005; Boyd et al., 2007; Marchetti et al., 2012; Smetacek et al., 2012; Cohen et al., 2018; Moreno et al., 2018). In iron-limited ecosystems, where the competitive ability of diatoms has been extensively investigated, they succeed through a combination of rapid iron uptake (Shaked et al., 2005; McQuaid et al., 2018), storage of excess iron (Lampe et al., 2018), and economizing on iron usage. Iron plays essential roles in cellular growth and metabolism due to its use in both the

photosynthetic electron transport chain and construction of photosystems (Behrenfeld & Kolber, 1999; Blankenship, 2002; Lommer et al., 2012; Muhseen et al., 2015; Strzepek et al., 2011).

Diatoms have multiple strategies to reduce iron demand, many focused around the photosynthetic systems since the bulk of cellular iron in diatoms is used in iron-rich protein complexes including Photosystem I and II and the cytochrome b_6f complex. (Timmermans & Wagt, 2010; Strzepek et al., 2011; Lommer et al., 2012; Muhseen et al., 2015; Moreno et al., 2018). *Thalassiosira pseudonana*, a model coastal diatom, downregulates genes involved in the production of photosynthetic proteins, cytochrome b_6f, and ATP synthase under iron limitation (Nunn et al., 2013). Similar responses were found in a transcriptomic study on *Thalassiosira oceanica*, a diatom that lives in oligotrophic waters (Lommer et al., 2012). Some iron stressed diatoms substitute iron-free flavodoxin for ferritin or use copper-containing plastocyanin instead of cytochrome b_6f (La Roche et al., 1996; Boyd et al., 1999; Erdner et al., 1999; Peers & Price, 2006; Raven, 2013; Moreno et al., 2018).

While these aforementioned acclimations to low iron involve modifications to conventional photosynthetic pathways, it has also been suggested that iron-stressed diatoms may instead generate energy via proteorhodopsin (PR), a light driven proton pump that lacks iron (Marchetti et al., 2015). PR is a member of the rhodopsin family, a group of proteins with either light-driven ion pumping or visual sensory functions (Spudich et al., 2000; Fuhrman et al., 2008). All rhodopsin proteins, regardless of function, contain a retinal chromophore bound to 7 transmembrane helices (Béjà et al., 2000; Marchetti et al., 2015). When the chromophore absorbs light, the protein experiences structural shifts that result in either signal transduction or transport of ions through the membrane (Spudich, 2006; Vader et al., 2018). Bacteriorhodopsin, a proton pumping variant of rhodopsin, was discovered in 1971 in the halophilic archaea *Halobacterium*

salinarum (Oesterhelt & Stoeckenius, 1971; Béjà et al., 2001). Further study of the protein revealed that archaea may use the proton-pumping ability of bacteriorhodopsin to build a membrane potential used to power ATP synthase (Danon & Stoeckenius, 1974; Béjà et al., 2001).

A second proton pumping variant of rhodopsin was subsequently discovered in the bacterial clades SAR86 and SAR11 (Mullins et al., 1995; Béjà et al., 2001; Giovannoni et al., 2005). This form of rhodopsin was called proteorhodopsin due to its discovery in γ-*Proteobacteria* (Béjà et al., 2000). The presence of PR in these abundant and widely distributed clades suggested that PR plays a much more influential role in the microbial processing of energy and carbon than previously thought (Béjà et al., 2000, 2001). It was initially believed to be used only by heterotrophic organisms, considering that photo-autotrophs already have a mechanism to harvest energy from light (Giovannoni et al., 2005). As research on PR continued, it was discovered in nearly every taxon, including autotrophic eukaryotes, and environment in the world, solidifying its position as a severely understudied energy pathway relative to its prevalence in the marine environment (Torre et al., 2003; Giovannoni et al., 2005; McCarren & DeLong, 2007; Frias-Lopez et al., 2008; Bamann et al., 2014; Vader et al., 2018).

A metatranscriptomic study in the northeastern Pacific Ocean found a rhodopsin-like gene was upregulated during iron limitation in diatoms while photosynthetic proteins were downregulated (Marchetti et al., 2012). Further study into the rhodopsin-like gene revealed that it coded for PR and was typically found in species of diatoms that grow in cold, HNLC regions of the ocean (Marchetti et al., 2015). Together these findings suggest that chronically iron stressed diatoms in cold climates may use PR to generate energy when photosynthetic processes have been downregulated. Considering that the molecular makeup of PR contains no iron and its

reaction rate is not slowed by low temperatures, it seems to be an excellent technique of coping with decreased energy generation due to iron limitation (Marchetti et al., 2015; Pinhassi et al., 2016).

Although several lines of evidence support the claim that PR is involved in the iron limitation response in certain diatoms, the quantitative significance of energy generation via PR compared to the conventional photosynthetic pathway is not known. In an effort to illuminate what portion of a diatom's energy may be generated through PR rather than photosynthesis and how that ratio may change with iron stress, an energy budget has been constructed for the PR-containing diatom *Pseudo-nitzschia subcurvata* under both iron replete and iron limited conditions. The *P. subcurvata* strain investigated here was isolated from the Southern Ocean and is representative of the pennate diatoms that respond to transient iron addition in the Southern Ocean and other HNLC regions (Boyd et al., 2007). Changes in photosynthetic energy fluxes under increasing iron stress were also investigated in *P. subcurvata* and compared with responses of two Southern Ocean diatoms that lack PR to identify potential signatures of PR-supported energy generation.

METHODS

Diatom Culturing

Three Antarctic diatoms were used in the following experiments: one PR containing diatom and two non-PR containing diatoms for comparison. The PR containing diatom, *Pseudo-nitzschia subcurvata* (UNC1901), is a pennate diatom collected from Palmer LTER station 200.040. The two non-PR containing diatoms, *Synedra spp.* (UNC 1904) and *Chaetoceros socialis* (UNC1905), a pennate and a centric diatom respectively, were also isolated from Palmer LTER 200.040.

Culturing techniques closely followed those of Cohen et al., (2018). Media preparation and maintenance of Antarctic diatoms employed trace metal clean techniques following the description in Marchetti et al., (2006). Cultures were grown in Aquil media (Price et al., 1989). Synthetic ocean water (SOW) was prepared with additions of 300 µmol L^{-1} nitrate, 100 µmol L^{-1} silicate, and 10 µmol L^{-1} phosphate. The SOW was filtered through a Chelex 100 resin aiding in removal of transition ions from the seawater to ensure no iron contamination was present. One hundred µmol L^{-1} of 0.2-µm filtered ethylenediaminetetraacetic acid (EDTA) and trace metal mix were then added to the media along with cobalamin, thiamine, and biotin at Aquil concentrations. Samples for proteomics were grown under 4 iron concentrations.

The iron replete (pFe 19.0) samples were grown in Aquil media with an addition of 1370 nmol L^{-1} total iron (Fe_T), one level of iron limitation (pFe 21.65) contained 3.1 nmol L^{-1} Fe_T and the other (pFe 21.95) 1.5 nmol L^{-1} Fe_T. pFe values are defined as $-\log[Fe^{3+}]$ (W. Sunda et al., 2005). The final and most iron limiting treatment utilized 3.5 nmol L^{-1} Fe_T with 400 nM desferroxiamine B (DFB), a strong iron chelator. Samples for oxygen production, carbon

fixation, and photosynthesis vs irradiance measurements were grown under the same conditions however, due to time constraints, the pFe 21.65 treatment was excluded.

The cultures were maintained at 4°C under a light intensity of 100 µmol photons m^{-2} s^{-1} in 30 mL tubes at exponential phase. For the experiments, cultures were grown in acid-washed 1 L polycarbonate bottles to achieve greater biomass. Growth phase was tracked using a Turner 10-AU fluorometer. The cells for proteomics were collected in mid-exponential phase on a 3.0-µm polycarbonate filter and kept at -20°C until extraction.

The extent of iron limitation was measured using a Satlantic Fluorescence Induction and Relaxation (FIRe) fluorometer. F_v/F_m values approximate the ability of photosystem II (PSII) to direct light energy into the photosynthetic system. Decreased F_v/F_m values suggested lowered functioning of photosynthetic structures, and therefore, higher iron limitation (Greene et al., 1991; Behrenfeld & Milligan, 2013). Sigma values approximate the size of the PSII antennae. Antennae size tends to increase under iron limitation as it increases the chances of the cells absorbing photons used to power the photosynthetic system. Subsamples were exposed to blue light (450 nm) for 100 µs providing estimates of F_o and F_m values. The equation $(F_m-F_o)F_m^{-1}$ was used to calculate F_v:F_m.

Photosynthetic Rates

Energy flow through the photosynthetic pathway was constrained at three different points: oxygen production by photosystem II, electron transport between the photosystems, and carbon fixation in the dark reactions. By measuring activity at three separate points, a more holistic picture of photosynthetic efficiency was generated.

Oxygen Production Measurements

Rates of gross oxygen production and respiration in the light were measured using an $^{18}O_2$ assay and a membrane inlet mass spectrometer (MIMS) as outlined in Kana (1992). The method relies on the fact that O_2 production from water-splitting at PSII generates effectively only $^{16}O_2$ whereas respiration consumes $^{16}O_2$ and $^{18}O_2$ in direct proportion to their concentrations in solution.

To estimate oxygen production, 400 mL of culture were concentrated via gentle filtration (< 5 in. Hg) and resuspended in 1.3 mL of medium before being added to the MIMS chamber. The MIMS chamber rested above a membrane covered inlet that allows for passage of dissolved gases into the mass spectrometer. The samples were stirred at 300 rpm using a magnetic stir bar and maintained at 4°C by water bath. Any O_2 gas initially present in the culture was removed by gently bubbling N_2 gas into the sample. Once a majority of the O_2 gas had been removed, a cover was placed over the chamber to prevent gas exchange between the sample and the atmosphere. After depletion of natural O_2 present in the sample, a 0.5 mL bubble of $^{18}O_2$ was added by syringe and allowed to exchange with the solution. The gas exchange was stopped by removing the $^{18}O_2$ bubble when the $^{18}O_2$ concentration reached a value similar to the oxygen concentration originally present in the culture.

Photosynthesis was induced by shining a light into the sample of the same intensity at which they were grown under (100 µmol photons m^{-2} s^{-1}). Respiration in the light was determined from the rate of $^{18}O_2$ consumption and the ratio of $^{18}O_2$ to $^{16}O_2$ in the MIMS chamber. Gross oxygen production was estimated by the rate of change of $^{16}O_2$, which is the only isotope of oxygen produced by photosynthesis (Radmer & Ollinger, 1980), and correcting for the respiration rate in the light. The light was then turned off so the rate of respiration in the dark

could also be measured as the total O_2 ($^{18}O_2$ + $^{16}O_2$) loss rate. All rates were normalized to cell number. These productivity estimates were then converted to energy fluxes by using the Gibbs free energy of the water splitting reaction, estimated as 237 kJ mol^{-1} in standard state conditions (Greenbaum, 1988; Renger, 2011).

Carbon Fixation Measurements

Gross carbon fixation rates were measured using a ^{14}C-DIC tracer approach following protocols described in Shen & Hopkinson (2015). Fifty mL of culture was mixed with 4 µCi of ^{14}C-HCO_3 and incubated for 2 hours at 4°C at growth irradiance. To measure total ^{14}C activity, 200 µL of the assay was placed into a scintillation vial with 400 µL of betaphenethylamine and 10 mL of scintillation fluid. To measure ^{14}C fixed by the algae, the remainder of the sample was filtered onto a 1.2 µm polycarbonate filter and placed into a scintillation vial with 1 mL of 1% HCl to remove any residual ^{14}C-DIC. The solution was allowed to degas overnight before 10 mL of scintillation fluid was added. Twenty-four hours later both samples were counted on a liquid scintillation counter. Rates of C-fixation were calculated from the ^{14}C incorporated and the specific activity determined from the total ^{14}C activity and the total DIC in solution which was assumed to be 2.0 mM. The carbon fixation rates were converted to energy fluxes using the Gibbs free energy of carbon fixation, 479 kJ mol^{-1} (Johnson, 2016).

Electron Transport Measurements

Photosynthetic electron transport rates were measured as a function of incident irradiance using a FIRe fluorometer. The photosynthesis versus irradiance (PvE) curves so obtained provide additional constraints on the integrated response of photosynthetic physiology to iron stress and serve as an additional proxy for photosynthetic efficiency. PvE curves show the changing rate of

photosynthesis as light irradiances increase. The initial slope of the curve, α, represents the cells' ability to utilize low light levels. As light irradiance increases, the curve flattens out and reaches a stable, maximal value. The highest point of the curve, Pmax, shows the highest rate of photosynthesis achieved under the varying light levels.

The PvE curves were generated using the FIRe fluorometer equipped with a calibrated, actinic light source that allowed irradiance to be controlled during measurements of chlorophyll fluorescence. Photosynthetic electron transport (ETR) rates were calculated from fluorescence measurements using a modified version of the relationship proposed in equation 1 (Kolber & Falkowski, 1993):

$$\mathrm{ETR} = \sigma_{PS2} * q_P(E) * \mathrm{n}_{PS2} * \mathrm{f} * E \quad (1)$$

Where σ_{PS2} is the PS2 antenna size, q_p is the fraction of open reaction centers at a given irradiance, n_{PS2} is the number of chlorophyll a molecules per PS2, f is the fraction of functional PS2 reaction centers (calculated as the dark-adapted F_v/F_m divided by 0.65), and E is the irradiance. All the parameters can be determined from FIRe data except n_{PS2}, which is assumed to be 500, following Kolber & Falkowski, (1993). Table 1.1 contains descriptions of FIRe parameters used to the create PvE curves found in this experiment.

Table 1.1: Fluorescence Induction and Relaxation System parameters for building photosynthesis vs irradiance curves.

Parameter	**Setting**
Single-Turnover Flash (STF)	200 µs
Multiple-Turnover Flash (MTF)	200 ms
Photosynthetically Available Radiation (PAR)	200 µmol m^{-2} s^{-1}
PAR Off Interval	0 s
PAR On Interval	2 s

Estimating Energy Flux through Proteorhodopsin

Energy flow through proteorhodopsin was estimated by quantifying the abundance of PR per cell with quantitative, targeted mass spectrometry-based proteomics. The parallel reaction monitoring (PRM) method was used to target PR associated peptides allowing for absolute quantification (Peterson et al., 2012).

Protein Extraction and Purification

Protein (membrane and cytosolic fractions) was extracted and purified following a procedure adapted from Gallagher & Waldbauer (2020). Diatom cells were lysed via probe sonication in 333 µL of wash solution (50 mM Tris-HCl, pH 7.5) and cell debris was removed by centrifugation at 2500x g for 8 minutes. The supernatant, containing proteins, was removed and mixed with 830 µL of carbonate extraction solution (100 mM sodium carbonate). The samples were shaken at 4°C for 1 hr. In order to increase the likelihood of isolating PR, a membrane-bound protein, the samples were spun in an ultracentrifuge at 115,000x g for 1 hr resulting in a cytosolic fraction and a pelleted membrane fraction. The membrane fraction was resuspended by probe sonication in 150 µL of LDS buffer (0.333 g Tris HCl, 0.341 g Tris Base, 0.400 g LDS, 0.006 g EDTA, 4 g glycerol in 10 mL MilliQ-grade water). The samples were then incubated for 20 min at 95° C and 30 mins at 37° C. The total protein was then quantified using a Pierce BCA Assay (ThermoFisher). After quantification, the samples were reduced with 10 mM DTT for 1 hr at RT and then alkylated in 60 nM iodoacetamide for 1 hr at RT in the dark.

The extracted proteins were then purified and digested with eFASP (enhanced filter aided sample preparation; (Erde et al., 2014)). In order to separate the leftover chemicals and unwanted biomolecules from the proteins, 50 µL of lysate and 400 µL of exchange buffer (8M urea, 0.2%

(w/v) deoxycholate, 1M ammonium bicarbonate) were added onto a 10,0000 MWCO HY concentrator and spun down at 14,000x g for 30 mins into a passivated collection tube (Erde et al., 2017). This step was repeated until all of the lysate had been added to the filter. The filter was washed 3 times with 200 µL of exchange buffer and then washed 2 times in 200 µL of digestion buffer (50 mM ammonium bicarbonate with 0.2% (w/v) deoxycholate). The proteins were digested overnight at RT on the filter in 100 µL of digestion buffer and 2 µg of trypsin. After overnight digestion, the mixture was spun down eluting digested peptides into the collection tube. The filter was rinsed twice with 50 µL of peptide recovery buffer (50 mM ammonium bicarbonate) to ensure no peptides were left on the filter. The filtrate was added to 200 µL of ethyl acetate and 2.5 µL of TFA before being gently vortexed. The tubes were filled with ethyl acetate and sonicated for 10 s in a water bath. The mixture was spun down at 14,000x g for 10 minutes and the resultant organic layer removed. This was done 3 times. The sample was then heated to 60° C for 5 minutes uncovered to remove residual ethyl acetate before being dried down in a vacuum centrifuge and frozen at -20°C until MS analysis. Once ready to be analyzed, the samples were resuspended in 5% acetonitrile and spiked with 5 nM of heavy labelled synthetic peptide.

Predicted Proteome

A predicted proteome for *P. subcurvata* was previously generated by collaborators from an assembled transcriptome. The transcriptome was sequenced and assembled using the Trinity assembler following procedures described in Moreno et al. 2018. The corresponding proteome was predicted from the transcriptome using GeneMarkS-T (Tang et al., 2015) and its quality and completeness were assessed with BUSCO v3 using the Eukaryotic protein set (Seppey et al.,

2019). The BUSCO analysis showed the proteome was reasonably complete with 83.2% of the expected core proteins being completely (54.5%) or partially (28.7%) identified. A single proteorhodopsin candidate protein was identified by blastp homology with PR sequences from other diatoms (Marchetti et al., 2015).

Mass Spectrometric Analysis – Targeted Method

The mass spectrometry analyses were performed on a Thermo-Fisher LTQ Orbitrap Elite Mass Spectrometer coupled with a Proxeon Easy NanoLC system (Waltham, MA) located at the Proteomics and Mass Spectrometry Facility, University of Georgia. The enzymatic peptides were loaded into a reversed-phase column (self-packed column/emitter, 0.1x~150 mm ID, with 200 Å 5 µM Bruker MagicAQ C18 resin), then directly eluted into the mass spectrometer at a flow rate of 450 nL/min. Briefly, the two-buffer gradient elution (0.1% formic acid as buffer A and 99.9% acetonitrile with 0.1% formic acid as buffer B) starts with 0% B, holds at 0%B for 2 minutes, then increases to 10% B in 35 minutes, to 25% B in 60 minutes, to 50% B in 25 min and to 95% B in 10 minutes.

The parallel reaction monitoring (PRM) method was carried out by constantly scanning the m/z ranges (a window of 2 Thomson) where 4 ions of interest associated with the chosen peptides are expected (Peterson et al., 2012). MS scans were acquired by Orbitrap at the resolutions of 120,000 and 15,000, respectively. The targeted peptides are listed in Table 1.2.

Table 1.2: List of peptides of interest used in targeted mass spectrometry. Unlabeled peptides represent the natural concentration of proteorhodopsin in the samples. Labelled peptides were added to the samples in a known concentration.

Targeted Peptides	Associated Protein	m/z	Modifications
LPADESR	Proteorhodopsin	394.2	NA
LPADES(R)	Proteorhodopsin	399.2	^{13}C and ^{15}N labelled Arginine
VPSVHEK	Proteorhodopsin	398.2	NA
VPSVHE(K)	Proteorhodopsin	402.2	^{13}C and ^{15}N labelled Lysine

Protein Quantification by AQUA

The absolute PR concentration in molecules cell^{-1} was estimated using the AQUA procedure (Gerber et al., 2003). Heavy-labelled peptides are used to build an internal standard by adding a known concentration of each heavy peptide to the samples of native "light" peptides. Two tryptic peptides specifically associated with PR that resolve well in the MS were chosen to become quantitative markers. These peptides were synthetically created (HeavyPeptide, ThermoFisher) and labelled with ^{15}N and ^{13}C on either arginine or lysine depending on the configuration of the peptide. Because the synthetic and natural peptides only differ in mass, they behave the same way in the LC-MS system allowing for direct comparison between the signal intensity of the peptides. The quantity of PR in each sample can be determined from the ratio of known concentration of the synthetic peptide to the signal intensity of the synthetic peptide. This ratio was determined using Skyline, an open-source program used to evaluate quantitative proteomics experiments (MacLean et al., 2010). Once this ratio is calculated, the concentration of PR in mols cell^{-1} can be estimated by back-calculating using the total number of cells in the sample.

Energy flux through the proteorhodopsin pathway was estimated by measuring the abundance of PR protein in samples of *P.* subcurvata using targeted, quantitative mass-spectrometry based proteomics. PR abundance was converted to energy flux using equations 2 and 3. Protein abundance (*PR)*, turnover rate (τ), and proton stoichiometry (S_{H^+}) were multiplied to generate proton flux. Turnover rate represents the amount of time it takes a molecule of PR to pump a proton across the membrane. Proton stoichiometry refers to the number of protons that are transported per each photon absorbed by the molecule. This flux was then multiplied by the free energy across the cytoplasmic membrane, ΔG, to produce energy flux. Values for τ, S_{H^+}, ΔG and were taken to be 20 s^{-1} (Wang et al. 2003) , 1 (Stoeckenius & Bogomolni, 1982), and 18 kJ mol^{-1} respectively, based on available literature values.

$$H^+flux\ (mol\ cell^{-1}s^{-1}) = PR * \tau * S_{H^+} \quad (2)$$

$$Energy\ flux\ (mol\ cell^{-1}s^{-1}) = \Delta G * H^+flux \quad (3)$$

Semi-Quantitative Analysis by Spectral Counting

Spectral counting was used to determine relative changes in protein abundance under varying iron concentrations. In spectral counting methods, each mass spectrum is assigned to a peptide and then a protein. The spectral count is the total number of mass spectra identified for a protein. By examining the change in this value, a semi-quantitative picture of changing protein abundance can be created (Lundgren et al., 2010; Nunn et al., 2013).

Spectral counts were generated via the Trans-Proteomic Pipeline (TPP) developed by the Seattle Proteome Center. TPP is an open-source program that can be used to transform, analyze, and statistically verify the results produced from tandem mass spectrometry experiments in one

environment (Deutsch et al., 2010). The raw data was searched by SEQUEST against the predicted proteome for *P. subcurvata.* Peptides were identified using Peptide Prophet and assigned to proteins using Protein Prophet. The resulting spectral counts were normalized accounting for the length of each protein (NSAF) (Zybailov et al., 2006; Cohen et al., 2018).The NSAF scores were then analyzed using the statistical PLGEM package available for R to determine proteins that were significantly differentially expressed under different iron treatments (Pavelka et al., 2004, 2008).

RESULTS

Iron Limitation and Growth

P. subcurvata was grown under three different iron treatments: iron replete (pFe 19.0: 1370 nmol L^{-1} iron), low iron (pFe 21.95: 3.2 nmol L^{-1} iron), and with a strong chelator, DFB, intended to induce strong iron limitation (DFB: 3.2 nmol L^{-1} iron with 400 nmol L^{-1} DFB). Only in the DFB treatment was growth rate significantly reduced from iron replete conditions (Fig. 2.1), but F_v/F_m progressively decreased as iron bioavailability was reduced (Fig. 2.2) and sigma progressively increased (Fig. 2.3). Taken together these results show iron stress was strong enough to induce physiological changes in the *P. subcurvata* cultures, with progressively stronger physiological effects as iron bioavailability was reduced. *C. socialis* was grown under two iron treatments: iron replete (pFe 19.0) and low iron (pFe 21.95). Neither growth rate (Fig 2.1) nor F_v/F_m (Fig 2.2) was affected by iron treatment, but sigma increased at low iron (Fig. 2.3), indicating modest effects of iron on cellular physiology. *Synedra spp.* was grown under two iron treatments: iron replete (pFe 19.0) and DFB. The DFB treatment significantly reduced growth rate (Fig 2.1) and F_v/F_m (Fig 2.2) and increased sigma (Fig. 2.3), the combination of which indicates strong physiological effects of iron limitation.

Energy Generation by Conventional Photosynthesis

There was a tendency for gross and net oxygen production to decrease as the strength of iron limitation increased in all phytoplankton species (Fig 2.4). In *P. subcurvata*, gross oxygen production decreased in both pFe 21.95 and DFB treatments compared to pFe 19.0 conditions.

However, net oxygen production was only statistically significantly different from iron replete conditions in the DFB treatment, possibly due to high variability among replicates. In *C. socialis*, gross oxygen production was significantly reduced at low iron (pFe 21.95) but net oxygen production was not affected. In *Synedra* spp., gross and net oxygen production were both reduced under the DFB treatment.

Carbon fixation rates were measured via ^{14}C-DIC incorporation for each species. Carbon fixation rates showed the same trend as oxygen production in that it decreased with increasing iron limitation (Fig 2.5). Carbon fixation in *P. subcurvata* was reduced under the pFe 21.95 treatment relative to the pFe 19.0 treatment and was suppressed even further under the DFB treatment. *C. socialis* and *Synedra spp.* both significantly decreased rates of carbon fixation under reduced iron bioavailability.

Rates of photosynthetic electron transport were calculated as a function of irradiance, generating PvE curves and estimates of electron transport rates at growth irradiance. These curves provided estimates of α and Pmax. Each species showed an increase in α as they experienced more extreme iron limitation (Fig 2.6). In general, iron limitation is associated with decreased rates of Pmax across all three species (Fig 2.7).

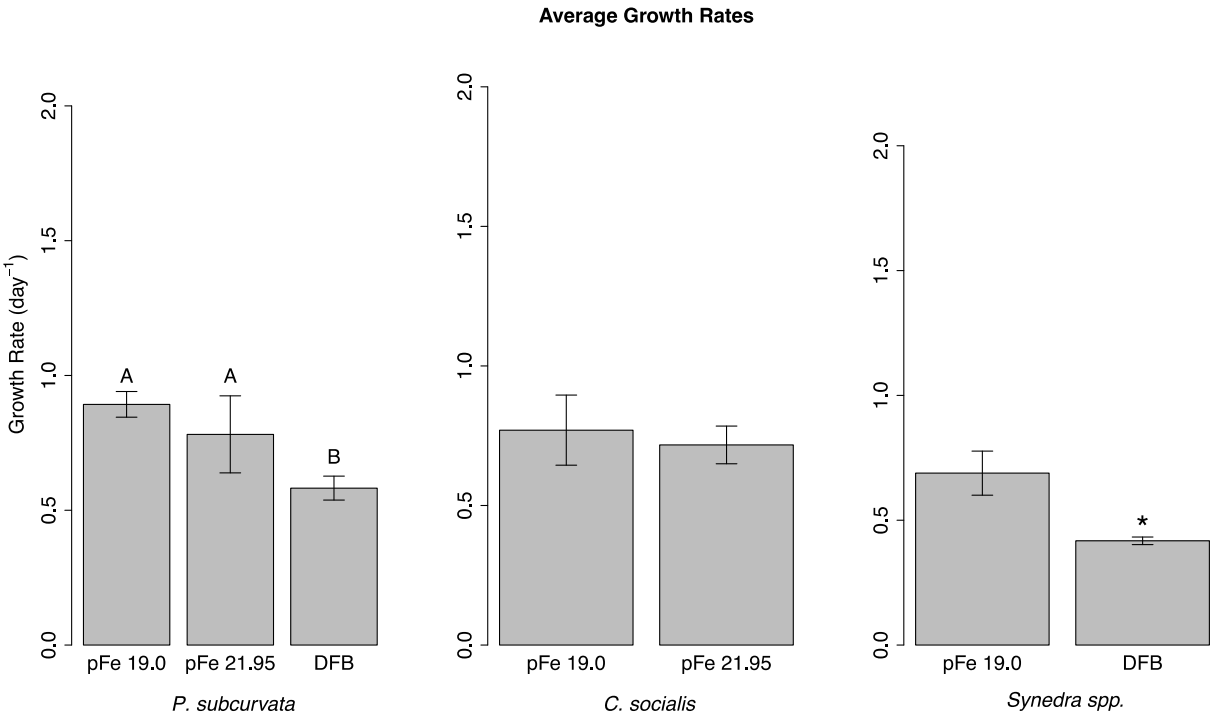

Figure 2.1: Average growth rates measured by fluorescence. Error bars represent one standard deviation. Bars marked with the same letter are not significantly different from each other. An asterisk represents values that are significantly different from the corresponding pFe 19.0 value for the same species.

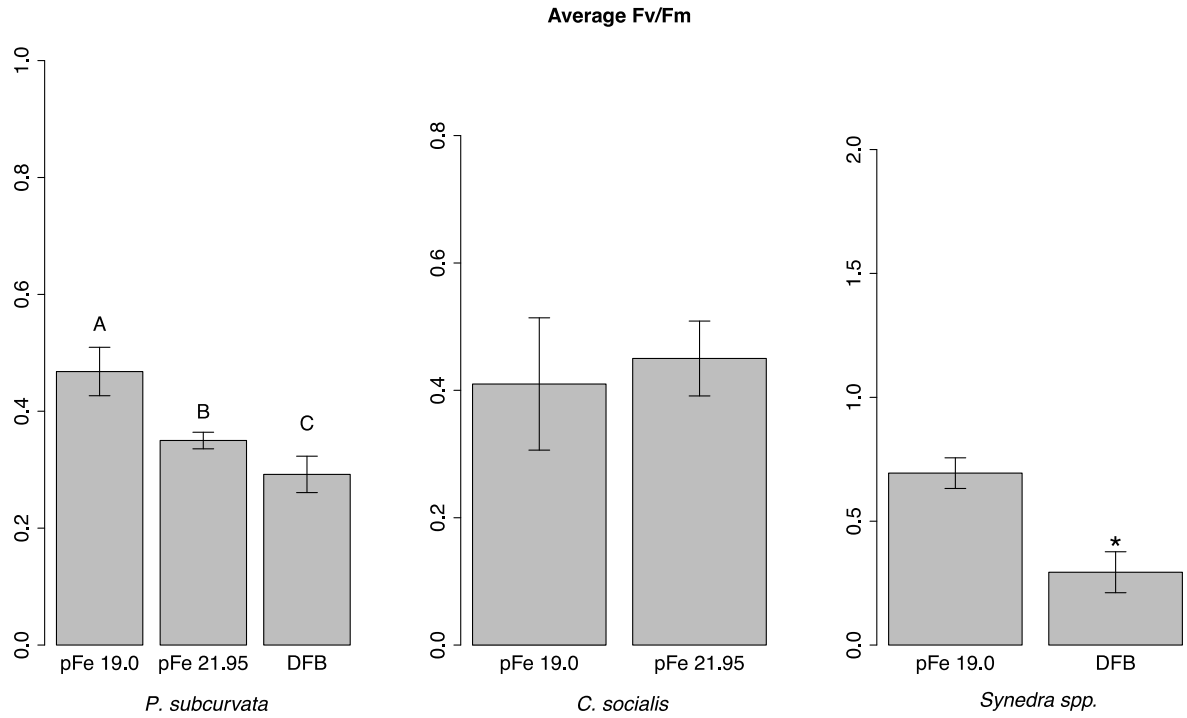

Figure 2.2: Average Fv/Fm for each iron treatment across all measured species. Cultures were not dark adapted before being measured. Error bars represent one standard deviation. Bars marked with the same letter are not significantly different from each other. An asterisk represents values that are significantly different from the corresponding pFe 19.0 value for the same species.

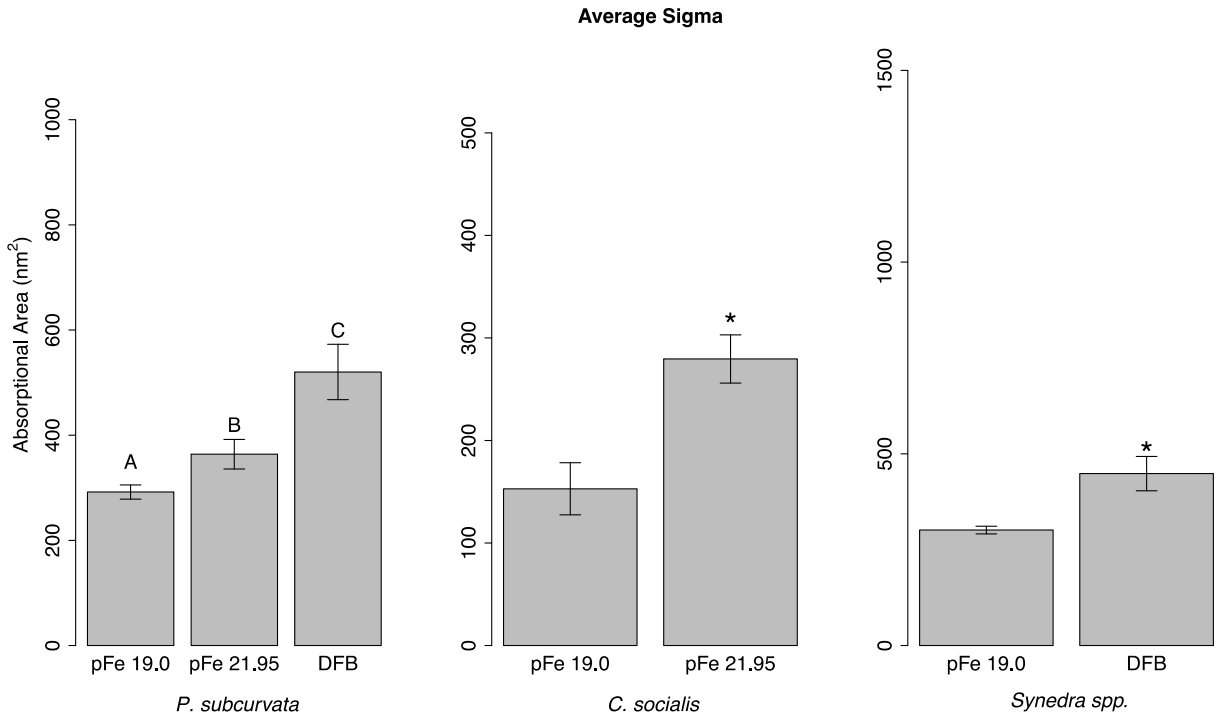

Figure 2.3: Average sigma for each iron treatment across all measured species. Cultures were not dark adapted before being measured. Error bars represent one standard deviation. Bars marked with the same letter are not significantly different from each other. An asterisk represents values that are significantly different from the corresponding pFe 19.0 value for the same species.

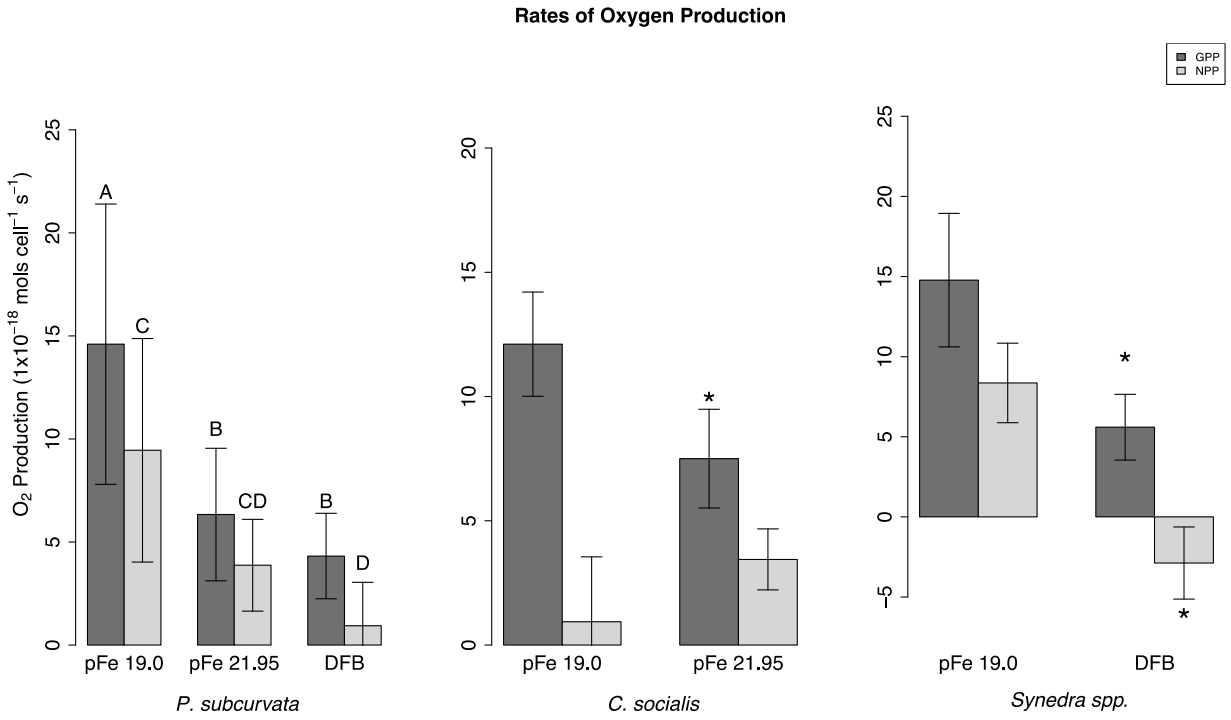

Figure 2.4: Gross primary production (black) and net primary production (gray) as rates of oxygen production. Error bars represent one standard deviation. Y-axes are not on the same scale. Units are reported at a magnitude of $x10^{-18}$. Bars marked with the same letter are not significantly different from each other. Statistical differences were not analyzed between gross and net values (C and D are not necessarily different from A and B). An asterisk represents values that are significantly different from the corresponding pFe 19.0 value for the same species.

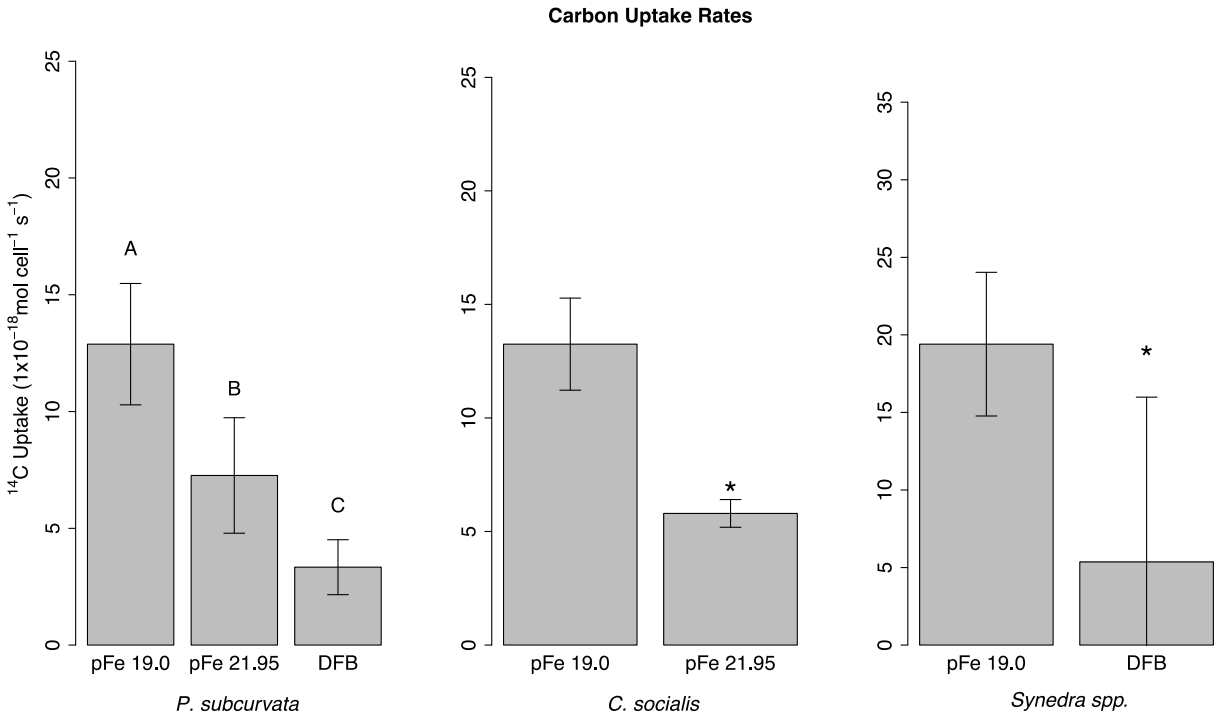

Figure 2.5: Average rates of carbon uptake for each iron treatment across all measured species. Error bars represent one standard deviation. Y-axes are not on the same scale. Units are reported at a magnitude of x10^{-18}. Bars marked with the same letter are not significantly different from each other. An asterisk represents values that are significantly different from the corresponding pFe 19.0 value for the same species.

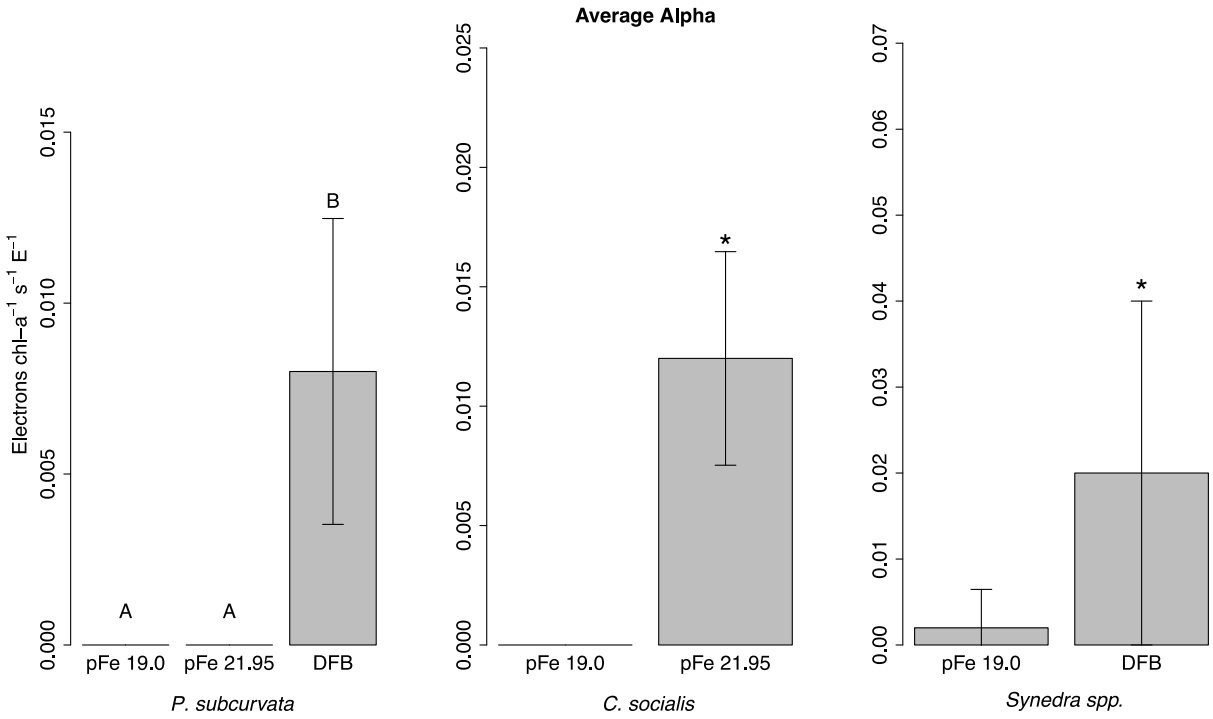

Figure 2.6: Values for α under each iron treatment across all measured species. Error bars represent one standard deviation. Y-axes are not set to the same scale. Bars marked with the same letter are not significantly different from each other. An asterisk represents values that are significantly different from the corresponding pFe 19.0 value for the same species.

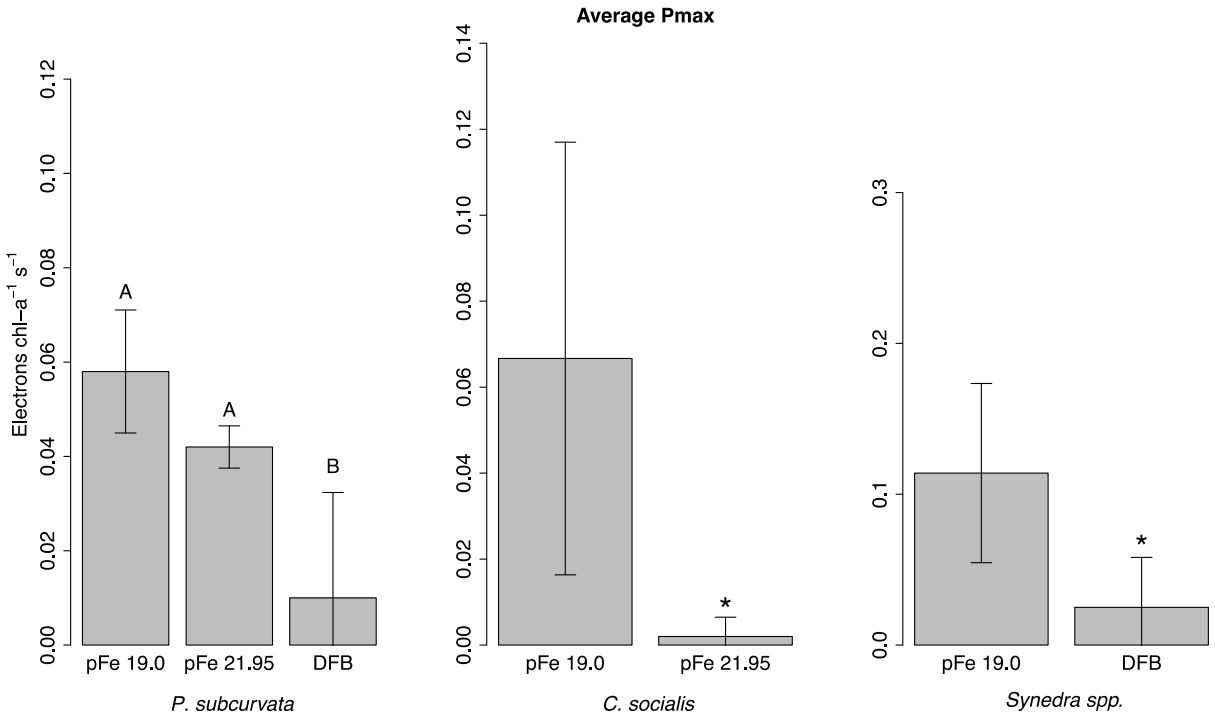

Figure 2.7: Pmax is plotted for each iron treatment across all measured species. Error bars represent one standard deviation. Bars marked with the same letter are not significantly different from each other. An asterisk represents values that are significantly different from the corresponding pFe 19.0 value for the same species.

Measurements of Proteorhodopsin

Iron Limitation and Growth

P. subcurvata cultures for proteomic analysis were grown under the same three iron treatments as listed in the previous section (pFe 19.0, pFe 21.95, and DFB) with the addition of a second low iron treatment (pFe 21.65). The DFB treatment showed significant changes in growth rate (Fig 2.8) and sigma (Fig 2.10) compared to the other three treatments. While Fv/Fm values steadily decreased with decreasing iron bioavailability (Fig 2.9), the pFe 21.95 and DFB treatments were not significantly distinct from each other. The two low iron treatments (pFe

21.65 and pFe 21.95) did not demonstrate statistically significant differences from each other for any measurement. Their Fv/Fm and sigma values remained distinct from the iron replete treatment (Fig 2.9 and 2.10), but their growth rates were similar to those of the iron replete treatment (Fig 2.8). This indicates the pFe 21.65 and pFe 21.95 treatments display a moderate level of iron stress while the DFB treatment can be considered physiologically distinct from the iron replete treatment.

Energy Flux through PR

Protein abundance was used to estimate maximum values of energy flux through PR in *P. subcurvata* cultures. Two unique, tryptic peptides (LPADESR and VPSVHEK) were chosen as markers for PR allowing for absolute quantification of the protein. Energy fluxes through the proteorhodopsin pathway show an apparent increase with increasing iron stress. High variability in the mass spectrometric measurements may have affected the statistical analysis of energy flux measurements possibly explaining the discrepancies in statistical significances between the two peptides (LPADESR and VPSVHEK; Table 2.1). Energy flux through PR increased significantly from the pFe 19.0 and pFe 21.65 treatments to the DFB treatment when quantifying with the VPSVHEK peptide (Fig 2.11). Analyzing the LPADESR peptide reveals no statistical significances despite the qualitative upward trend of energy flux with increasing iron limitation (Fig 2.11).

Changes in Protein Expression

Spectral counting techniques and PLGEM statistical analysis were used to examine changes in protein expression between the pFe 19.0 and DFB treatments of *P. subcurvata*. Proteins with good functional annotations, based on BLAST homology to proteins of known function, and that were both: 1) substantially (2x) up- or down-regulated and 2) statistically significantly different ($p < 0.05$) between iron treatments were examined. Several light harvesting complex proteins (LHC 1-4), which bind pigments that capture light for photosynthesis, and components of photosystem II (PsbU, PsbV, OEC) were highly downregulated under extreme iron stress (Fig. 2.13). In contrast, an iron starvation protein (ISIP), an NADPH oxido-reductase, and PR were identified as being significantly upregulated under low iron bioavailability (Fig 2.13).

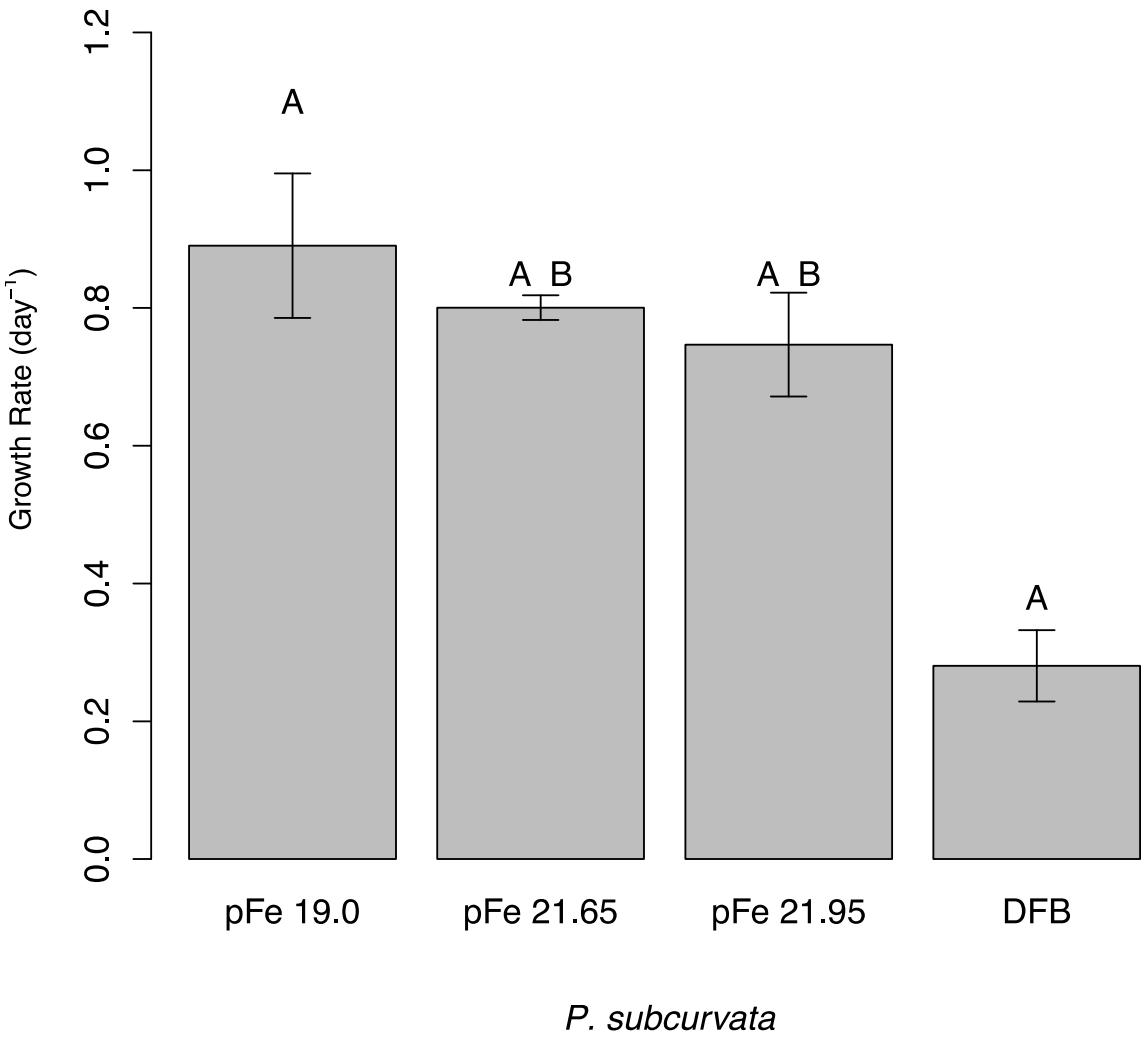

Figure 2.8: Average growth rates measured by fluorescence. Error bars represent one standard deviation. Bars marked with the same letter are not significantly different from each other.

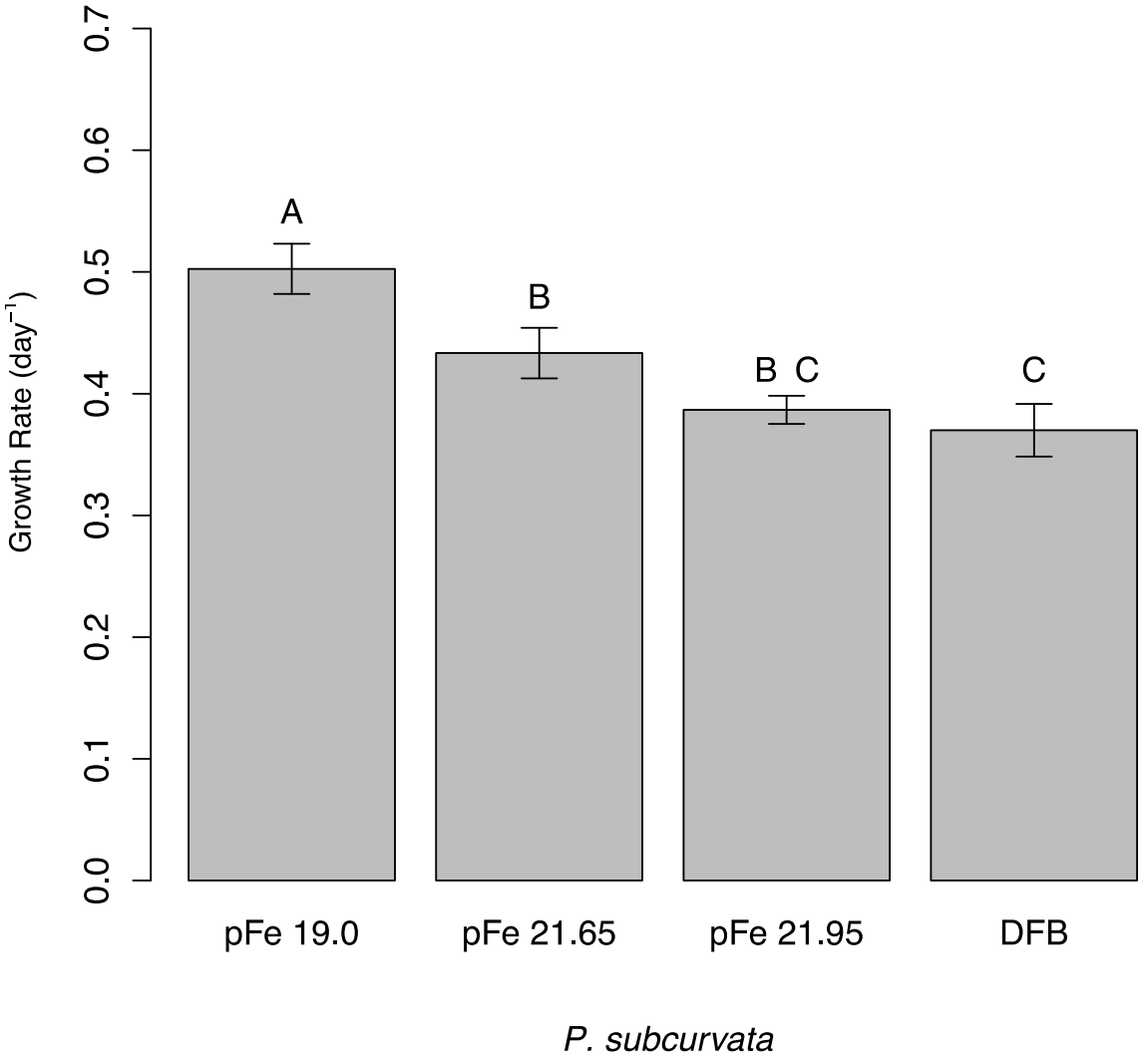

Figure 2.9: Average Fv/Fm measured by FIRe. Error bars represent one standard deviation. Bars marked with the same letter are not significantly different from each other.

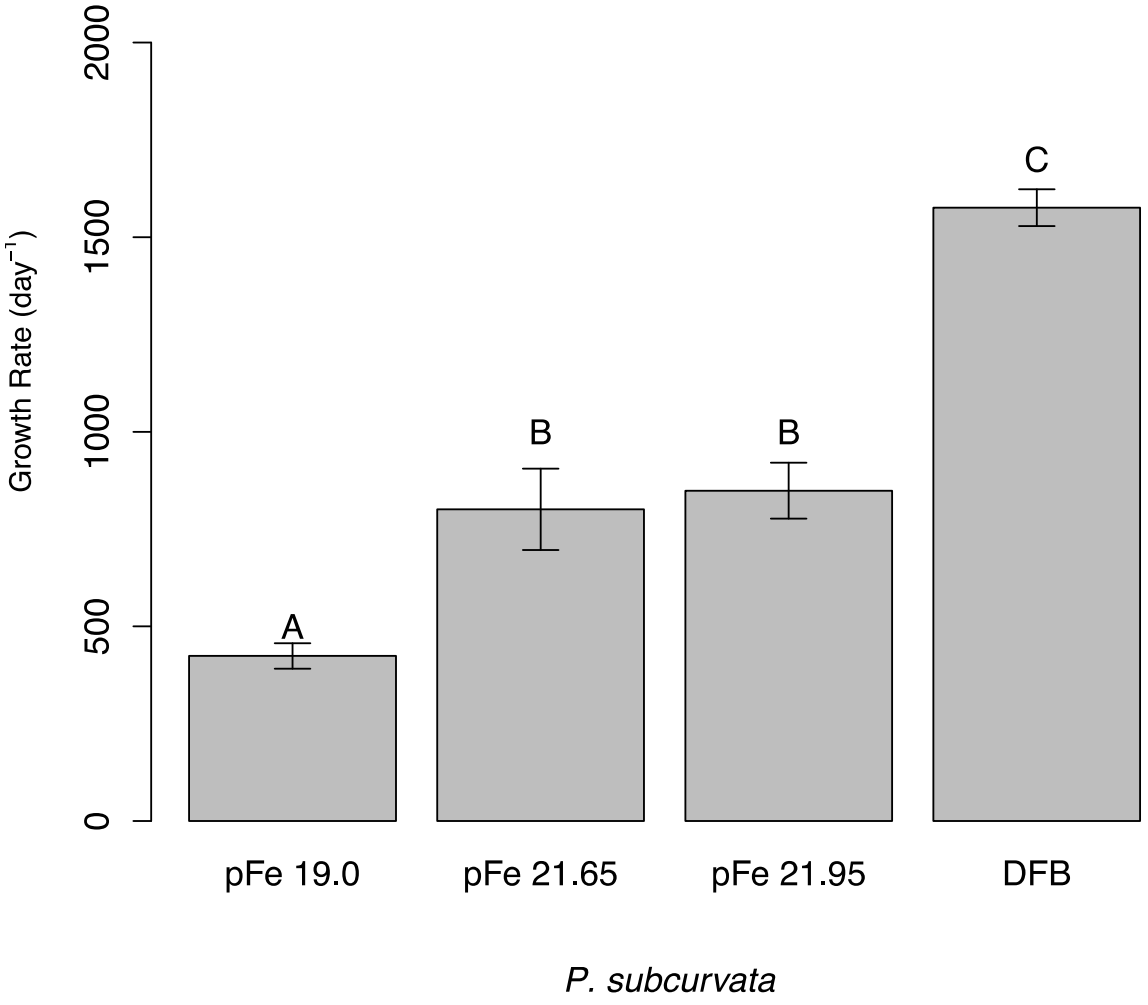

Figure 2.10: Average sigma measured by FIRe. Error bars represent one standard deviation. Bars marked with the same letter are not significantly different from each other.

Table 2.1: Significant differences between iron treatments for energy flux values (kJ $cell^{-1}$ s^{-1}) were determined by ANOVA followed by Tukey's Honest Significant Differences test. Significance is denoted by an asterisk and defined as a p-value less than 0.5 or a 95% confidence interval that does not include 0.

LPADESR	**p-value**	**95% Confidence Interval**
pFe 19.0, DFB	0.15	$-3.18 \times 10^{-18} – 4.41 \times 10^{-19}$
pFe 21.65, DFB	0.12	$-3.26 \times 10^{-18} – 3.65 \times 10^{-19}$
pFe 21.95, DFB	0.29	$-2.89 \times 10^{-18} – 7.30 \times 10^{-19}$
pFe 21.65, pFe 19.0	0.99	$-1.89 \times 10^{-18} – 1.74 \times 10^{-18}$
pFe 21.95, pFe 19.0	0.95	$-1.53 \times 10^{-18} – 2.10 \times 10^{-18}$
pFe 21.95, pFe 21.65	0.91	$-1.45 \times 10^{-18} – 2.18 \times 10^{-18}$
VPSVHEK	**p-value**	**95% Confidence Interval**
pFe 19.0, DFB	0.02*	$-5.99 \times 10^{-19} – -5.46 \times 10^{-20}$*
pFe 21.65, DFB	0.04*	$-5.53 \times 10^{-19} – -8.54 \times 10^{-21}$*
pFe 21.95, DFB	0.18	$-4.67 \times 10^{-19} – 7.77 \times 10^{-20}$
pFe 21.65, pFe 19.0	0.95	$-2.26 \times 10^{-19} – 3.18 \times 10^{-19}$
pFe 21.95, pFe 19.0	0.45	$-1.40 \times 10^{-19} – 4.05 \times 10^{-19}$
pFe 21.95, pFe 21.65	0.75	$-1.86 \times 10^{-19} – 3.59 \times 10^{-19}$

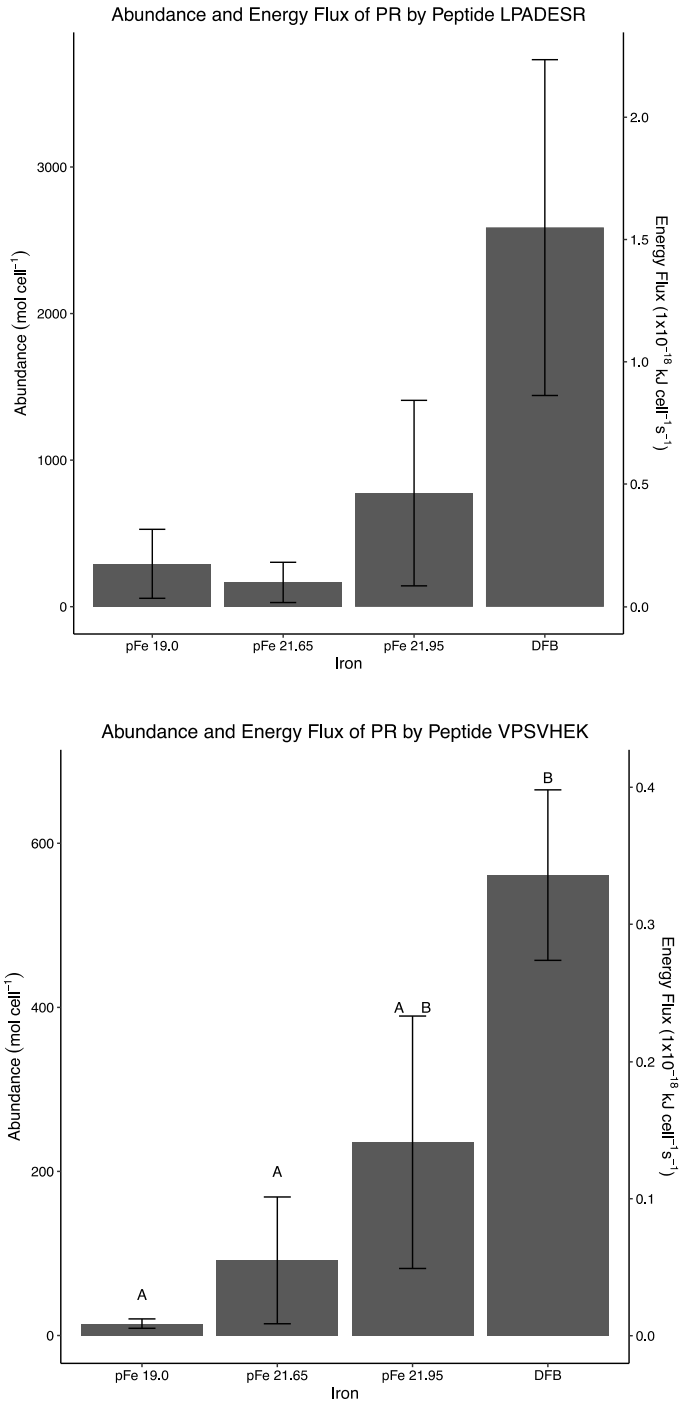

Figure 2.11: Average energy fluxes through PR by LPADESR and VPSVHEK. Error bars represents one standard error from the mean. Units are reported at a magnitude of $1x10^{-18}$ kJ/cell/s.

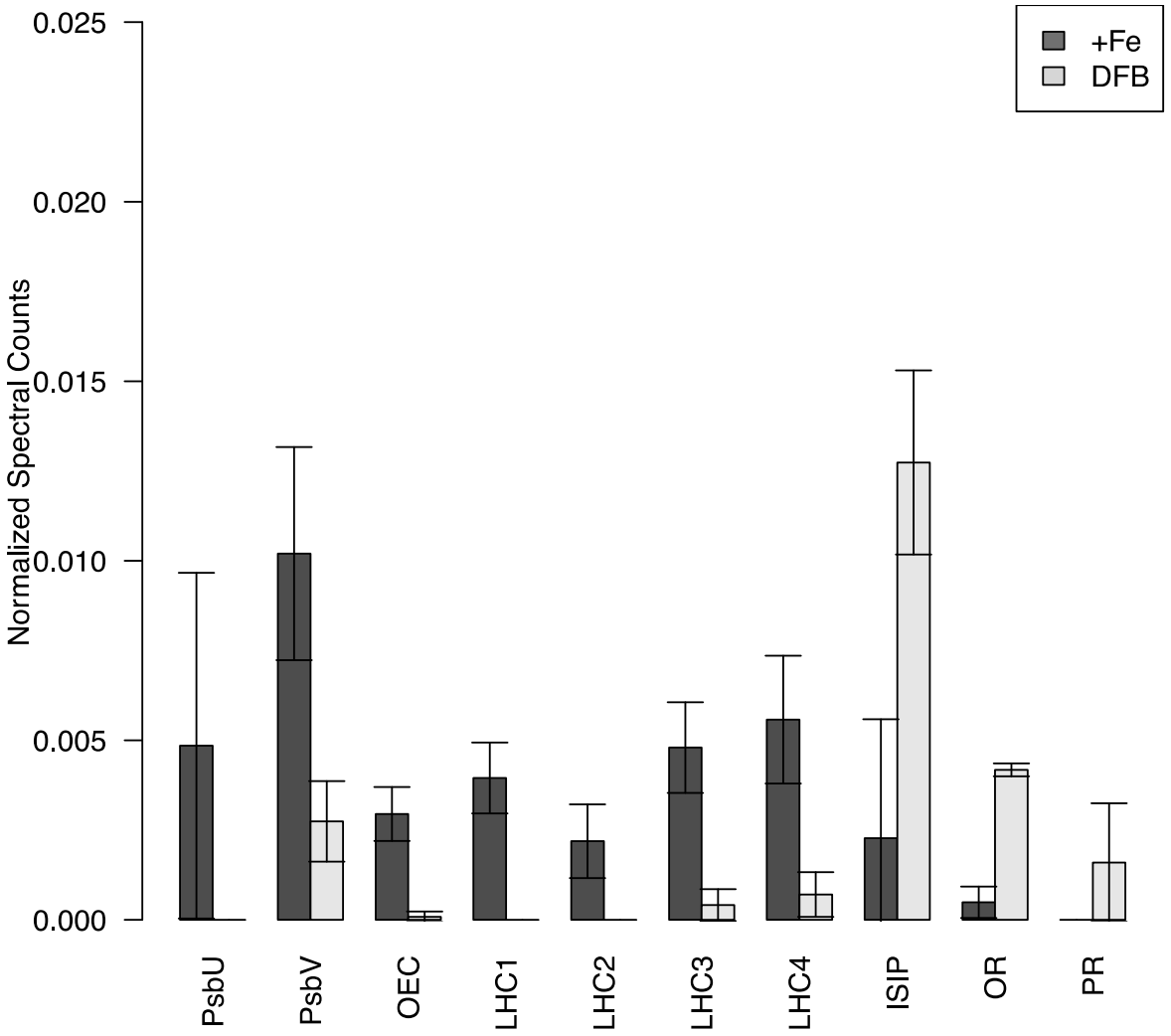

Figure 2.13: Normalized spectral counts for 10 significantly differentially expressed photosynthesis related proteins. One error bar represents one standard deviation. The proteins are components of photosystem II (PsbU, PsbV, OEC), light harvesting complexes (LHC1-4), an iron starvation induced protein (ISIP), an NADHP oxido-reductase (OR), and proteorhodopsin (PR).

DISCUSSION

Photosynthetic organisms generate both reducing power, as NADPH, and energy, as ATP, for carbon fixation and other cellular needs through the photosynthetic light reactions. However, linear electron flow through the photosynthetic systems does not produce sufficient ATP to support both carbon fixation and other metabolic needs relative to the amount of NADPH produced (Allen, 2002). Photoautotrophs have evolved several alternative strategies (Fig 3.1) to generate supplementary ATP including cyclic electron transport around PSI (Shikanai, 2007), water-water cycles (Asada, 1999; McDonald et al., 2011), and mitochondrial ATP generation (Bailleul et al., 2015). Because of the high iron requirement of PSI (12 iron atoms per complex), ATP generation mechanisms involving PSI are generally not used in marine autotrophs (Behrenfeld & Milligan, 2013), since iron is rarely plentiful in the ocean. Instead, marine phytoplankton are known to make use of PSII-based water-water cycles such as PTOX (Cardol et al., 2008; Mackey et al., 2008) or involve the mitochondria, as has been demonstrated for several species of marine diatoms (Bailleul et al., 2015). These mechanisms require less iron than PSI-based processes, but still require significant iron investments in PSII, oxidases, or electron transport, depending on the particular mechanism employed (Behrenfeld & Milligan, 2013). In contrast, PR contains no iron, and so could serve as an iron-free alternative mechanism to generate supplementary energy. We sought to test this hypothesis by quantifying the energy generated from PR in a Southern Ocean strain of *P. subcurvata*, analyzing protein expression under iron limited and non-limited conditions, and by comparing photophysiological

acclimations to iron stress in *P. subcurvata* with that of two non-PR containing Southern Ocean diatoms, *C. socialis* and *Synedra spp*.

As *P. subcurvata* was grown under increasing iron stress, PR protein abundance and energy generation increased (Fig 2.11) while flux through the conventional light reactions decreased as indicated by reductions in gross oxygen production from PSII (Fig 2.4) and reduced photosynthetic electron transport (Fig. 2.7). Decreases in flux through the photosynthetic light reactions accompanied by declines in carbon fixation rates (Fig 2.5) were expected since the main sink for NADPH and ATP generated in the light reactions is carbon fixation in the Calvin-Benson cycle. This and previous studies have demonstrated that a common response to iron limitation by diatoms is to downregulate their photosynthetic system in order to reduce the cell's need for iron (W. G. Sunda & Huntsman, 1995; Moreno et al., 2018). The fact that under iron replete conditions, gross oxygen production rates were statistically indistinguishable from carbon fixation rates (Fig 3.2 and 3.3), though with some variation, suggested that *P. subcurvata* does not make substantial use of water-water cycle activity, such as PTOX, to produce supplementary ATP. Like other diatoms, *P. subcurvata* may instead shuttle reducing power to the mitochondria to generate additional ATP (Bailleul et al., 2015), although many diatoms do have candidate genes for PTOX (Grouneva et al., 2011) and so may make use of a PTOX-based water-water cycle to some extent. The approximate 1:1 ratio between gross oxygen production and carbon fixation was maintained under iron-stress, arguing that water-water cycle activity remained low under all iron conditions. While PR abundance increased under iron stress, our estimates of energy generated from PR, calculated from its abundance, turnover rate, and typical transmembrane proton energy gradients, remained small relative to the energy generated in conventional photosynthesis (Fig 3.4). The fraction of cellular energy generated by PR remained

<1% under all conditions, precluding PR from providing the supplementary ATP necessary to support metabolism. Instead, it is likely that *P. subcurvata* generates supplemental ATP by shuttling NADPH to the mitochondria and perhaps to some extent via PTOX, regardless of iron availability.

Quantification of PR via quantitative proteomics presented some challenges. Two tryptic peptides specific to PR were chosen to act as quantitative markers for PR abundance, LPADESR and VPSVHEK. Though in principle these two peptides should be present in the same amount, and thus serve as redundant measures of PR, the peptide concentrations and inferred PR abundance differed by nearly an order of magnitude between the two peptides. This discrepancy could be due to the similar retention time between the two peptides. By co-eluting into the mass spectrometer, LPADESR may have been suppressing the signal from VPSVHEK causing VPSVHEK to underrepresent the abundance of PR in the sample. The transition ions associated with VPSVHEK were often missed by the mass spectrometer resulting in lower signal estimates. For this reason, the rest of the discussion will focus on the data collected using the peptide LPADESR.

Estimates of PR abundance in *P. subcurvata* range from less than 300 copies per cell under iron replete conditions to nearly 3,000 copies per cell in the DFB treatment (Fig 2.11). These estimates are much lower than those for heterotrophic bacteria which have been calculated to be within the range of 6,000 to 145,000 depending on oceanic region. The rate of energy flux through PR under the DFB treatment was estimated to be $1.5x10^{-18}$ kJ $cell^{-1}$ s^{-1}. This value generally agrees with estimates of total energy flux through microbial PRs *in situ* which were estimated to be between $6.50x10^{-19}$ and $1.31x10^{-17}$ kJ $cell^{-1}$ s^{-1} (Gómez-Consarnau et al., 2019). Analysis shows that the amount of energy generated by PR accounted for less than 0.01% of

total energy under iron replete conditions and increased nearly 10x to just under 0.1% of energy under extreme iron limitation (Fig 3.4). While there is evidence to suggest PR can provide enough energy to sustain heterotrophic bacteria in some regions of the ocean, it does not seem likely that PR could provide enough energy alone to sustain the necessary metabolic rates required of diatoms.

In addition to estimating PR's contribution to total energy generation, we sought to compare how photosynthetic energy flows and characteristics respond to iron stress in PR-containing and PR-lacking diatoms, looking for clues to PR's role in mitigating iron stress. The results show that the changes in photosynthetic fluxes in the PR containing diatom, *P. subcurvata* were very similar to those in the non-PR containing diatoms, *C. socialis* and *Synedra spp* (Fig 3.5). For *P. subcurvata*, rates of gross and net oxygen production, electron transport, and carbon fixation were significantly slower under iron-stressed conditions when compared to the iron replete conditions. For *C. socialis*, each part of the photosynthetic system, excluding net oxygen production, operated significantly more slowly when the cells were iron limited (Fig 3.5). *Synedra spp.* behaved in a very similar manner with reductions in all rates except oxygen consumption. While downregulation of photosynthetic processes under iron-limitation is not unexpected, we also examined changes in relative rates of photosynthetic fluxes and similarly found little difference between PR-containing and PR-lacking diatoms. Ratios of carbon fixation to gross oxygen production were ~1 in all species under iron replete conditions and that ratio was maintained under iron stress in *P. subcurvata*, *C. socialis*, and *Synedra* (Fig 3.3). Despite containing PR, it seems that *P. subcurvata* does not display notable differences in downregulation of photosynthesis compared to non-PR containing diatoms.

Overall, it appears that the changes in the conventional photosynthetic system of the PR containing diatom *P. subcurvata* were similar to those of non-PR containing *C. socialis* and *Synedra spp*. While energy flux through PR did increase with iron limitation, it never exceeded 1% of the total energy budget and it does not seem to have produced enough energy to allow for increased rates of carbon fixation compared to the non-PR containing diatoms. Further study is needed to elucidate the physiological purpose of PR in Antarctic diatoms. Recent work on localization suggests that PR is localized to cytoplasmic vacuoles, which may store nutrients and iron (Andrews and Marchetti, personal communication). Consequently, PR may serve a more limited role of acidifying these vacuoles or helping to generate a transmembrane energy gradient to support nutrient and iron import into the vacuole.

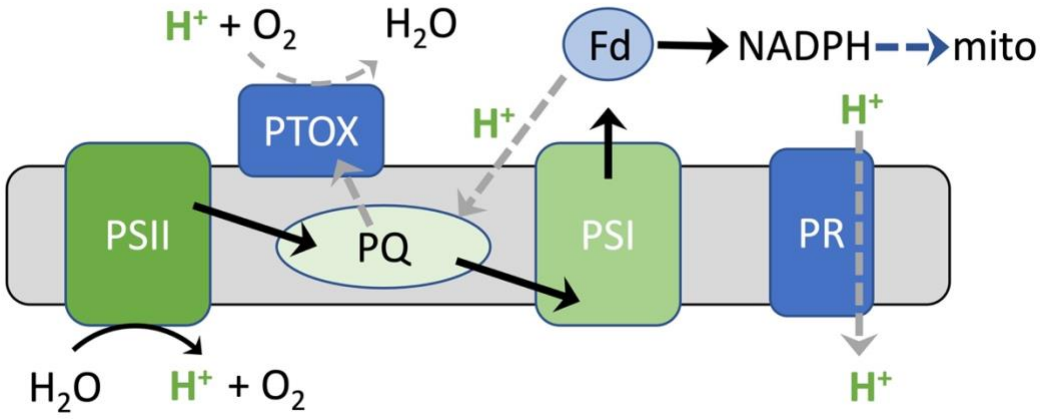

Fig. 3.1 Simplified diagram of linear electron flows (solid black arrows) through the photosynthetic light reactions (PSII – photosystem II, PQ – plastoquinone, PSI – photosystem I; Fd – ferredoxin) and alterative electron flows (dashed grey arrows) potentially used to generate supplemental energy in the form of a trans-thylakoid proton gradient that can be converted into ATP by ATP synthase (PTOX – plastoquinol terminal oxidase, Fd – ferredoxin, PR – proteorhodopsin). Note that the arrow from ferredoxin to plastoquinone is a simplified representation of PSI cyclic electron transport.

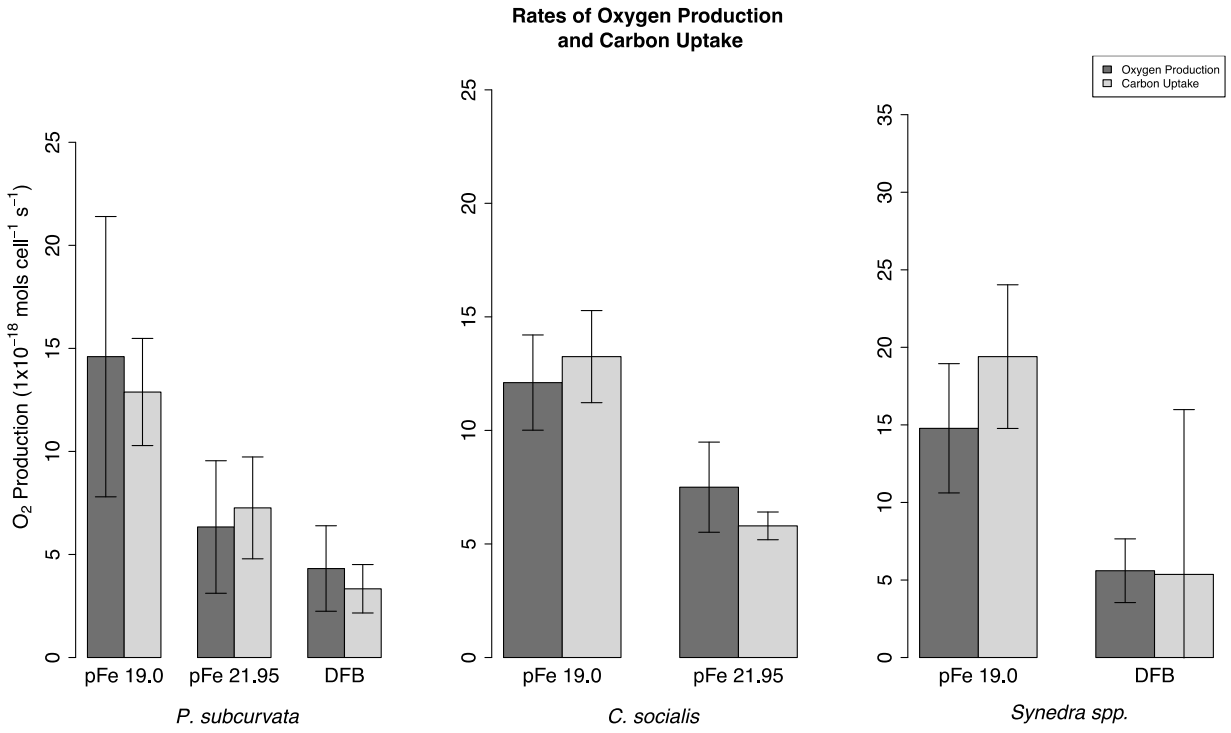

Figure 3.2: Bar graphs comparing rate of oxygen production to rate of carbon fixation. Both sets of measurements are reported in units of $x10^{-18}$. Error bars represent one standard deviation. Y-axes are not on the same scale.

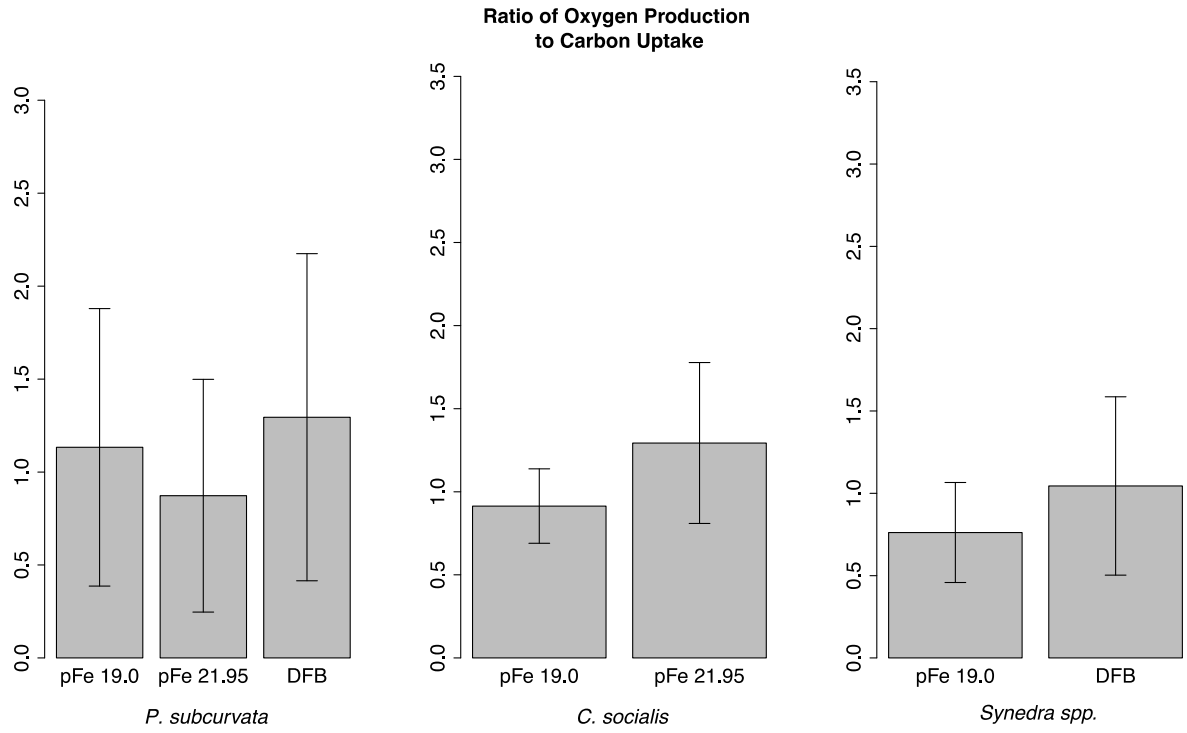

Figure 3.3: Bar graphs comparing ratio of oxygen production to carbon fixation. Both sets of measurements are reported at a scale of $1x10^{-18}$. Error bars represent one standard deviation calculated via propagation of error. Y-axes are not on the same scale.

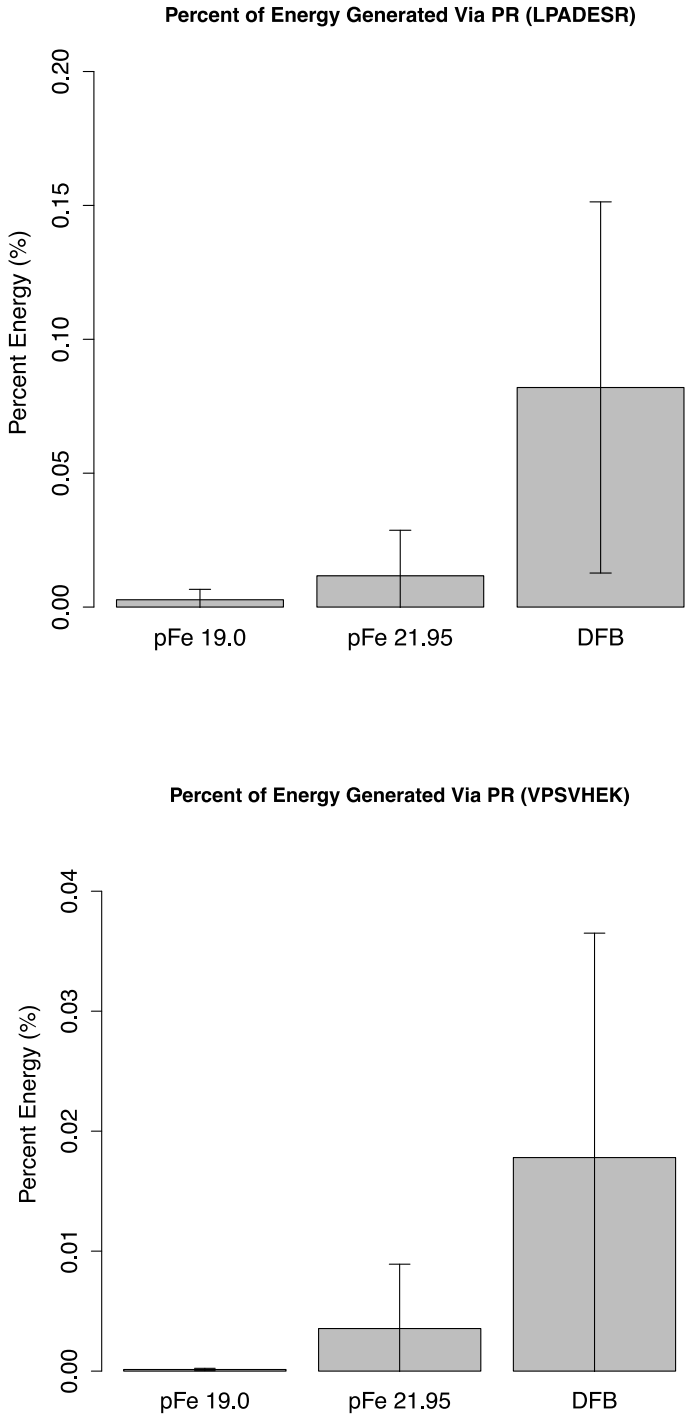

Figure 3.4: Percentage of total energy generated by PR calculated by quantifying peptide LPADESR and VPSVHEK. Error bars represents one standard deviation calculated via propagation of error.

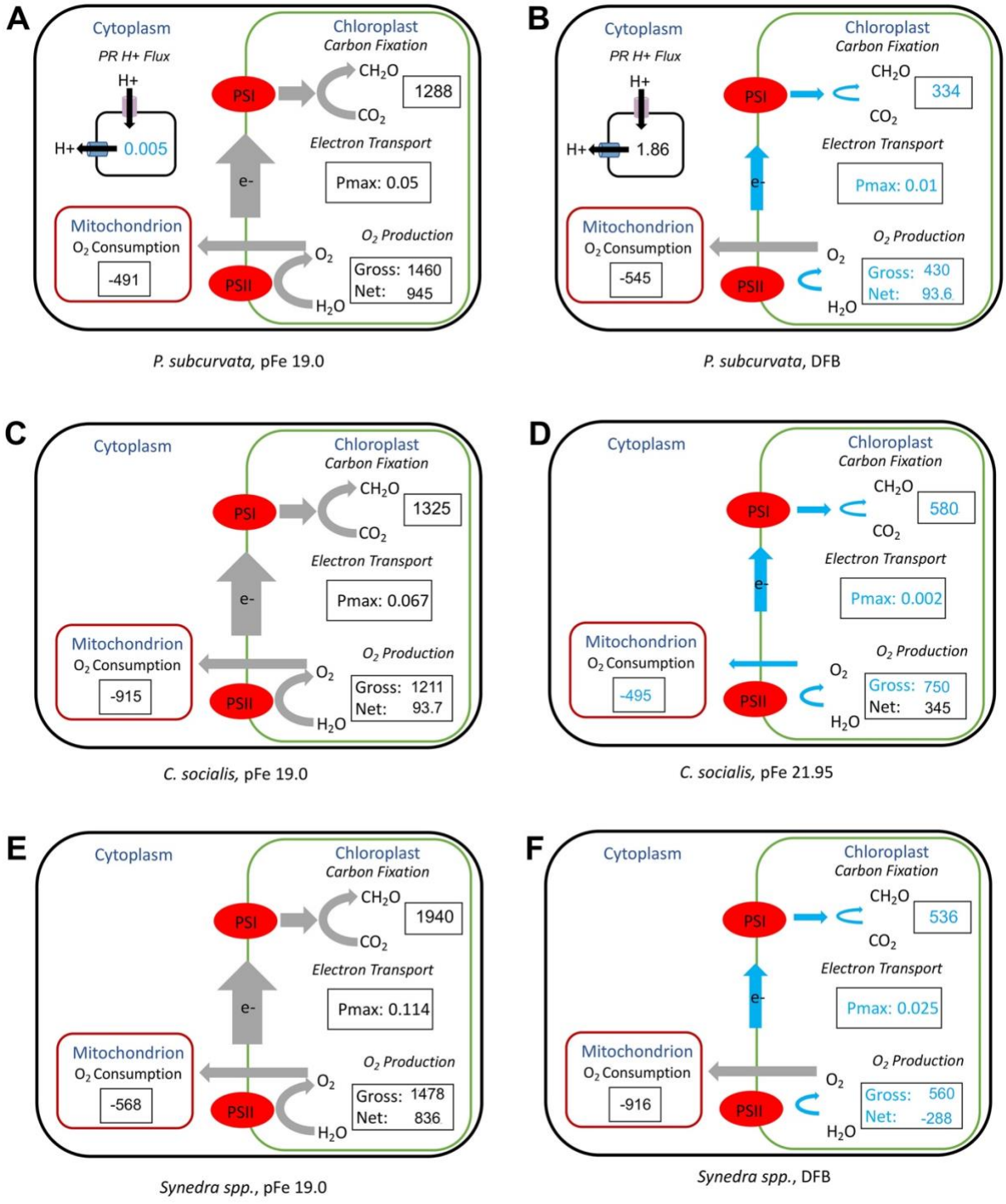

Figure 3.5 Diagrams representing major components of the cellular energy budget of three species of Southern Ocean diatoms (*P. subcurvata*: A, B; *C. socialis*: C, D; *Synedra spp.*: E, F) grown under iron replete (A, C, E) or iron-stressed (B, D, F) conditions. Values for oxygen production and consumption, carbon fixation, and hydrogen ion flux through PR are reported in units of $1x10^{-20}$ mol cell^{-1} s^{-1}. Pmax electron transport rates are represented in units of electrons

chl-a^{-1} s^{-1}. Blue coloring represents values that are significantly decreased when compared to the corresponding value of the treatment as determined by Student's t-test. Reported values for oxygen consumption were measured in the light.

REFERENCES

Allen, J. F. (2002). Photosynthesis of ATP—Electrons, Proton Pumps, Rotors, and Poise. *Cell*, *110*(3), 273–276. https://doi.org/10.1016/S0092-8674(02)00870-X

Arrigo, K. R. (2014). Sea Ice Ecosystems. *Annual Review of Marine Science*, *6*(1), 439–467. https://doi.org/10.1146/annurev-marine-010213-135103

Arrigo, K. R., Robinson, D. H., Worthen, D. L., Dunbar, R. B., DiTullio, G. R., VanWoert, M., & Lizotte, M. P. (1999). Phytoplankton Community Structure and the Drawdown of Nutrients and CO2 in the Southern Ocean. *Science*, *283*(5400), 365–367. https://doi.org/10.1126/science.283.5400.365

Asada, K. (1999). THE WATER-WATER CYCLE IN CHLOROPLASTS: Scavenging of Active Oxygens and Dissipation of Excess Photons. *Annual Review of Plant Physiology and Plant Molecular Biology*, *50*(1), 601–639. https://doi.org/10.1146/annurev.arplant.50.1.601

Bailleul, B., Berne, N., Murik, O., Petroutsos, D., Prihoda, J., Tanaka, A., Villanova, V., Bligny, R., Flori, S., Falconet, D., Krieger-Liszkay, A., Santabarbara, S., Rappaport, F., Joliot, P., Tirichine, L., Falkowski, P. G., Cardol, P., Bowler, C., & Finazzi, G. (2015). Energetic coupling between plastids and mitochondria drives CO 2 assimilation in diatoms. *Nature*, *524*(7565), 366–369. https://doi.org/10.1038/nature14599

Bamann, C., Bamberg, E., Wachtveitl, J., & Glaubitz, C. (2014). Proteorhodopsin. *Biochimica et Biophysica Acta (BBA) - Bioenergetics*, *1837*(5), 614–625. https://doi.org/10.1016/j.bbabio.2013.09.010

Behrenfeld, M. J., & Kolber, Z. S. (1999). Widespread Iron Limitation of Phytoplankton in the South Pacific Ocean. *Science, 283*(5403), 840–843. https://doi.org/10.1126/science.283.5403.840

Behrenfeld, M. J., & Milligan, A. J. (2013). Photophysiological Expressions of Iron Stress in Phytoplankton. *Annual Review of Marine Science*, *5*(1), 217–246. https://doi.org/10.1146/annurev-marine-121211-172356

Béjà, O., Aravind, L., Koonin, E. V., Suzuki, M. T., Hadd, A., Nguyen, L. P., Jovanovich, S. B., Gates, C. M., Feldman, R. A., Spudich, J. L., Spudich, E. N., & DeLong, E. F. (2000). Bacterial Rhodopsin: Evidence for a New Type of Phototrophy in the Sea. *Science*, *289*(5486), 1902–1906. https://doi.org/10.1126/science.289.5486.1902

Béjà, O., Spudich, E. N., Spudich, J. L., Leclerc, M., & DeLong, E. F. (2001). Proteorhodopsin phototrophy in the ocean. *Nature*, *411*(6839), 786–789. https://doi.org/10.1038/35081051

Blankenship, R. E. (2002). *Molecular Mechanisms of Photosynthesis*. John Wiley & Sons.

Boyd, P. W. (2002). The role of iron in the biogeochemistry of the Southern Ocean and equatorial Pacific: A comparison of in situ iron enrichments. *Deep Sea Research Part II: Topical Studies in Oceanography*, *49*(9), 1803–1821. https://doi.org/10.1016/S0967-0645(02)00013-9

Boyd, P. W., Jickells, T., Law, C. S., Blain, S., Boyle, E. A., Buesseler, K. O., Coale, K. H., Cullen, J. J., Baar, H. J. W. de, Follows, M., Harvey, M., Lancelot, C., Levasseur, M., Owens, N. P. J., Pollard, R., Rivkin, R. B., Sarmiento, J., Schoemann, V., Smetacek, V., … Watson, A. J. (2007). Mesoscale Iron Enrichment Experiments 1993-2005: Synthesis and Future Directions. *Science*, *315*(5812), 612–617. https://doi.org/10.1126/science.1131669

Boyd, P. W., LaRoche, J., Gall, M., Frew, R., & McKay, R. M. L. (1999). Role of iron, light, and silicate in controlling algal biomass in subantarctic waters SE of New Zealand. *Journal of Geophysical Research: Oceans*, *104*(C6), 13395–13408. https://doi.org/10.1029/1999JC900009

Cardol, P., Bailleul, B., Rappaport, F., Derelle, E., Béal, D., Breyton, C., Bailey, S., Wollman, F. A., Grossman, A., Moreau, H., & Finazzi, G. (2008). An original adaptation of photosynthesis in the marine green alga Ostreococcus. *Proceedings of the National Academy of Sciences*, *105*(22), 7881–7886. https://doi.org/10.1073/pnas.0802762105

Cohen, N. R., Gong, W., Moran, D. M., McIlvin, M. R., Saito, M. A., & Marchetti, A. (2018). Transcriptomic and proteomic responses of the oceanic diatom Pseudo-nitzschia granii to iron limitation. *Environmental Microbiology*, *20*(8), 3109–3126. https://doi.org/10.1111/1462-2920.14386

Danon, A., & Stoeckenius, W. (1974). Photophosphorylation in Halobacterium halobium. *Proceedings of the National Academy of Sciences*, *71*(4), 1234–1238. https://doi.org/10.1073/pnas.71.4.1234

de Baar, H. J. W., Boyd, P. W., Coale, K. H., Landry, M. R., Tsuda, A., Assmy, P., Bakker, D. C. E., Bozec, Y., Barber, R. T., Brzezinski, M. A., Buesseler, K. O., Boyé, M., Croot, P. L., Gervais, F., Gorbunov, M. Y., Harrison, P. J., Hiscock, W. T., Laan, P., Lancelot, C., … Wong, C.-S. (2005). Synthesis of iron fertilization experiments: From the Iron Age in the Age of Enlightenment. *Journal of Geophysical Research: Oceans*. https://doi.org/10.1029/2004JC002601@10.1002/(ISSN)2169-9291.HIGHCO2

Deutsch, E. W., Mendoza, L., Shteynberg, D., Farrah, T., Lam, H., Tasman, N., Sun, Z., Nilsson, E., Pratt, B., Prazen, B., Eng, J. K., Martin, D. B., Nesvizhskii, A., & Aebersold, R.

(2010). A Guided Tour of the Trans-Proteomic Pipeline. *Proteomics*, *10*(6), 1150–1159. https://doi.org/10.1002/pmic.200900375

Edwards, R., & Sedwick, P. (2001). Iron in East Antarctic snow: Implications for atmospheric iron deposition and algal production in Antarctic waters. *Geophysical Research Letters*, *28*(20), 3907–3910. https://doi.org/10.1029/2001GL012867

Erde, J., Loo, R. R. O., & Loo, J. A. (2014). Enhanced FASP (eFASP) to Increase Proteome Coverage and Sample Recovery for Quantitative Proteomic Experiments. *Journal of Proteome Research*, *13*(4), 1885–1895. https://doi.org/10.1021/pr4010019

Erde, J., Loo, R. R. O., & Loo, J. A. (2017). Improving Proteome Coverage and Sample Recovery with Enhanced FASP (eFASP) for Quantitative Proteomic Experiments. In L. Comai, J. E. Katz, & P. Mallick (Eds.), *Proteomics* (Vol. 1550, pp. 11–18). Springer New York. https://doi.org/10.1007/978-1-4939-6747-6_2

Erdner, D. L., Price, N. M., Doucette, G. J., Peleato, M. L., & Anderson, D. M. (1999). Characterization of ferredoxin and flavodoxin as markers of iron limitation in marine phytoplankton. *Marine Ecology Progress Series*, *184*, 43–53. https://doi.org/10.3354/meps184043

Falkowski, P. G. (1994). The role of phytoplankton photosynthesis in global biogeochemical cycles. *Photosynthesis Research*, *39*(3), 235–258. https://doi.org/10.1007/BF00014586

Frias-Lopez, J., Shi, Y., Tyson, G. W., Coleman, M. L., Schuster, S. C., Chisholm, S. W., & DeLong, E. F. (2008). Microbial community gene expression in ocean surface waters. *Proceedings of the National Academy of Sciences*, *105*(10), 3805–3810. https://doi.org/10.1073/pnas.0708897105

Fuhrman, J. A., Schwalbach, M. S., & Stingl, U. (2008). Proteorhodopsins: An array of physiological roles? *Nature Reviews Microbiology*, *6*(6), 488–494. https://doi.org/10.1038/nrmicro1893

Gallagher, G., & Waldbauer, J. (2020, February 20). *Proteome Expression in a Marine Photoheterotroph under Carbon and Nitrogen Limitation*. Ocean Sciences Meeting 2020. https://agu.confex.com/agu/osm20/meetingapp.cgi/Paper/647708

Gerber, S. A., Rush, J., Stemman, O., Kirschner, M. W., & Gygi, S. P. (2003). Absolute quantification of proteins and phosphoproteins from cell lysates by tandem MS. *Proceedings of the National Academy of Sciences*, *100*(12), 6940–6945. https://doi.org/10.1073/pnas.0832254100

Giovannoni, S. J., Bibbs, L., Cho, J.-C., Stapels, M. D., Desiderio, R., Vergin, K. L., Rappé, M. S., Laney, S., Wilhelm, L. J., Tripp, H. J., Mathur, E. J., & Barofsky, D. F. (2005). Proteorhodopsin in the ubiquitous marine bacterium SAR11. *Nature*, *438*(7064), 82–85. https://doi.org/10.1038/nature04032

Gómez-Consarnau, L., Raven, J. A., Levine, N. M., Cutter, L. S., Wang, D., Seegers, B., Arístegui, J., Fuhrman, J. A., Gasol, J. M., & Sañudo-Wilhelmy, S. A. (2019). Microbial rhodopsins are major contributors to the solar energy captured in the sea. *Science Advances*, *5*(8), eaaw8855. https://doi.org/10.1126/sciadv.aaw8855

Greenbaum, E. (1988). Energetic Efficiency of Hydrogen Photoevolution by Algal Water Splitting. *Biophysical Journal*, *54*(2), 365–368. https://doi.org/10.1016/S0006-3495(88)82968-0

Greene, R. M., Geider, R. J., & Falkowski, P. G. (1991). Effect of iron limitation on photosynthesis in a marine diatom. *Limnology and Oceanography*, *36*(8), 1772–1782. https://doi.org/10.4319/lo.1991.36.8.1772

Grouneva, I., Rokka, A., & Aro, E.-M. (2011). The Thylakoid Membrane Proteome of Two Marine Diatoms Outlines Both Diatom-Specific and Species-Specific Features of the Photosynthetic Machinery. *Journal of Proteome Research*, *10*(12), 5338–5353. https://doi.org/10.1021/pr200600f

Johnson, M. P. (2016). Photosynthesis. *Essays in Biochemistry*, *60*(3), 255–273. https://doi.org/10.1042/EBC20160016

Kana, T. M. (1992). Relationship Between Photosynthetic Oxygen Cycling and Carbon Assimilation in Synechococcus Wh7803 (cyanophyta)1. *Journal of Phycology*, *28*(3), 304–308. https://doi.org/10.1111/j.0022-3646.1992.00304.x

Kennedy, F., Martin, A., Bowman, J. P., Wilson, R., & McMinn, A. (2019). Dark metabolism: A molecular insight into how the Antarctic sea-ice diatom Fragilariopsis cylindrus survives long-term darkness. *New Phytologist*, *223*(2), 675–691.

Kolber, Z., & Falkowski, P. G. (1993). Use of active fluorescence to estimate phytoplankton photosynthesis in situ. *Limnology and Oceanography*, *38*(8), 1646–1665. https://doi.org/10.4319/lo.1993.38.8.1646

La Roche, J., Boyd, P. W., McKay, R. M. L., & Geider, R. J. (1996). Flavodoxin as an in situ marker for iron stress in phytoplankton. *Nature*, *382*(6594), 802–805. https://doi.org/10.1038/382802a0

Lampe, R. H., Mann, E. L., Cohen, N. R., Till, C. P., Thamatrakoln, K., Brzezinski, M. A., Bruland, K. W., Twining, B. S., & Marchetti, A. (2018). Different iron storage strategies

among bloom-forming diatoms. *Proceedings of the National Academy of Sciences*, *115*(52), E12275–E12284. https://doi.org/10.1073/pnas.1805243115

Levitus, S., Conkright, M. E., Reid, J. L., Najjar, R. G., & Mantyla, A. (1993). Distribution of nitrate, phosphate and silicate in the world oceans. *Progress in Oceanography*, *31*(3), 245–273. https://doi.org/10.1016/0079-6611(93)90003-V

Lommer, M., Specht, M., Roy, A.-S., Kraemer, L., Andreson, R., Gutowska, M. A., Wolf, J., Bergner, S. V., Schilhabel, M. B., Klostermeier, U. C., Beiko, R. G., Rosenstiel, P., Hippler, M., & LaRoche, J. (2012). Genome and low-iron response of an oceanic diatom adapted to chronic iron limitation. *Genome Biology*, *13*(7), R66.

Lundgren, D., Hwang, S., Wu, L., & Han, D. (2010). Role of spectral counting in quantitative proteomics. *Expert Review of Proteomics*, *7*, 39–53. https://doi.org/10.1586/epr.09.69

Luo, C.-S., Liang, J.-R., Lin, Q., Li, C., Bowler, C., Anderson, D. M., Wang, P., Wang, X.-W., & Gao, Y.-H. (2014). Cellular Responses Associated with ROS Production and Cell Fate Decision in Early Stress Response to Iron Limitation in the Diatom Thalassiosira pseudonana. *Journal of Proteome Research*, *13*(12), 5510–5523. https://doi.org/10.1021/pr5004664

Mackey, K. R. M., Paytan, A., Grossman, A. R., & Bailey, S. (2008). A photosynthetic strategy for coping in a high-light, low-nutrient environment. *Limnology and Oceanography*, *53*(3), 900–913. https://doi.org/10.4319/lo.2008.53.3.0900

MacLean, B., Tomazela, D. M., Shulman, N., Chambers, M., Finney, G. L., Frewen, B., Kern, R., Tabb, D. L., Liebler, D. C., & MacCoss, M. J. (2010). Skyline: An open source document editor for creating and analyzing targeted proteomics experiments. *Bioinformatics*, *26*(7), 966–968. https://doi.org/10.1093/bioinformatics/btq054

Marchetti, A., Catlett, D., Hopkinson, B. M., Ellis, K., & Cassar, N. (2015). Marine diatom proteorhodopsins and their potential role in coping with low iron availability. *The ISME Journal*, *9*(12), 2745–2748. https://doi.org/10.1038/ismej.2015.74

Marchetti, A., Maldonado, M. T., Lane, E. S., & Harrison, P. J. (2006). Iron requirements of the pennate diatom Pseudo-nitzschia: Comparison of oceanic (high-nitrate, low-chlorophyll waters) and coastal species. *Limnology and Oceanography*, *51*(5), 2092–2101. https://doi.org/10.4319/lo.2006.51.5.2092

Marchetti, A., Schruth, D. M., Durkin, C. A., Parker, M. S., Kodner, R. B., Berthiaume, C. T., Morales, R., Allen, A. E., & Armbrust, E. V. (2012). Comparative metatranscriptomics identifies molecular bases for the physiological responses of phytoplankton to varying iron availability. *Proceedings of the National Academy of Sciences*, *109*(6), E317–E325. https://doi.org/10.1073/pnas.1118408109

Martin, J. H. (1990). Glacial-interglacial CO2 change: The Iron Hypothesis. *Paleoceanography*, *5*(1), 1–13. https://doi.org/10.1029/PA005i001p00001

McCarren, J., & DeLong, E. F. (2007). Proteorhodopsin photosystem gene clusters exhibit co-evolutionary trends and shared ancestry among diverse marine microbial phyla. *Environmental Microbiology*, *9*(4), 846–858. https://doi.org/10.1111/j.1462-2920.2006.01203.x

McDonald, A. E., Ivanov, A. G., Bode, R., Maxwell, D. P., Rodermel, S. R., & Hüner, N. P. A. (2011). Flexibility in photosynthetic electron transport: The physiological role of plastoquinol terminal oxidase (PTOX). *Biochimica et Biophysica Acta (BBA) - Bioenergetics*, *1807*(8), 954–967. https://doi.org/10.1016/j.bbabio.2010.10.024

McQuaid, J. B., Kustka, A. B., Oborník, M., Horák, A., McCrow, J. P., Karas, B. J., Zheng, H., Kindeberg, T., Andersson, A. J., Barbeau, K. A., & Allen, A. E. (2018). Carbonate-sensitive phytotransferrin controls high-affinity iron uptake in diatoms. *Nature*, *555*(7697), 534–537. https://doi.org/10.1038/nature25982

Moore, J. K., Abbott, M. R., Richman, J. G., & Nelson, D. M. (2000). The Southern Ocean at the last glacial maximum: A strong sink for atmospheric carbon dioxide. *Global Biogeochemical Cycles*, *14*(1), 455–475.

Moreno, C. M., Lin, Y., Davies, S., Monbureau, E., Cassar, N., & Marchetti, A. (2018). Examination of gene repertoires and physiological responses to iron and light limitation in Southern Ocean diatoms. *Polar Biology*, *41*(4), 679–696. https://doi.org/10.1007/s00300-017-2228-7

Muhseen, Z. T., Xiong, Q., Chen, Z., & Ge, F. (2015). Proteomics studies on stress responses in diatoms. *PROTEOMICS*, *15*(23–24), 3943–3953. https://doi.org/10.1002/pmic.201500165

Mullins, T. D., Britschgi, T. B., Krest, R. L., & Giovannoni, S. J. (1995). Genetic comparisons reveal the same unknown bacterial lineages in Atlantic and Pacific bacterioplankton communities. *Limnology and Oceanography*, *40*(1), 148–158. https://doi.org/10.4319/lo.1995.40.1.0148

Nunn, B. L., Faux, J. F., Hippmann, A. A., Maldonado, M. T., Harvey, H. R., Goodlett, D. R., Boyd, P. W., & Strzepek, R. F. (2013). Diatom Proteomics Reveals Unique Acclimation Strategies to Mitigate Fe Limitation. *PLoS ONE*, *8*(10). https://doi.org/10.1371/journal.pone.0075653

Oesterhelt, D., & Stoeckenius, W. (1971). Rhodopsin-like Protein from the Purple Membrane of Halobacterium halobium. *Nature New Biology*, *233*(39), 149–152. https://doi.org/10.1038/newbio233149a0

Pavelka, N., Fournier, M. L., Swanson, S. K., Pelizzola, M., Ricciardi-Castagnoli, P., Florens, L., & Washburn, M. P. (2008). Statistical Similarities between Transcriptomics and Quantitative Shotgun Proteomics Data. *Molecular & Cellular Proteomics*, *7*(4), 631–644. https://doi.org/10.1074/mcp.M700240-MCP200

Pavelka, N., Pelizzola, M., Vizzardelli, C., Capozzoli, M., Splendiani, A., Granucci, F., & Ricciardi-Castagnoli, P. (2004). A power law global error model for the identification of differentially expressed genes in microarray data. *BMC Bioinformatics*, *5*(1), 203. https://doi.org/10.1186/1471-2105-5-203

Peers, G., & Price, N. M. (2006). Copper-containing plastocyanin used for electron transport by an oceanic diatom. *Nature*, *441*(7091), 341–344. https://doi.org/10.1038/nature04630

Peters, E., & Thomas, D. N. (1996). Prolonged darkness and diatom mortality I: Marine Antarctic species. *Journal of Experimental Marine Biology and Ecology*, *207*(1), 25–41. https://doi.org/10.1016/S0022-0981(96)02520-8

Peterson, A. C., Russell, J. D., Bailey, D. J., Westphall, M. S., & Coon, J. J. (2012). Parallel Reaction Monitoring for High Resolution and High Mass Accuracy Quantitative, Targeted Proteomics. *Molecular & Cellular Proteomics*, *11*(11), 1475–1488. https://doi.org/10.1074/mcp.O112.020131

Pinhassi, J., DeLong, E. F., Béjà, O., González, J. M., & Pedrós-Alió, C. (2016). Marine Bacterial and Archaeal Ion-Pumping Rhodopsins: Genetic Diversity, Physiology, and

Ecology. *Microbiology and Molecular Biology Reviews*, *80*(4), 929–954. https://doi.org/10.1128/MMBR.00003-16

Price, N. M., Harrison, G. I., Hering, J. G., Hudson, R. J., Nirel, P. M. V., Palenik, B., & Morel, F. M. M. (1989). Preparation and Chemistry of the Artificial Algal Culture Medium Aquil. *Biological Oceanography*, *6*(5–6), 443–461. https://doi.org/10.1080/01965581.1988.10749544

Radmer, R., & Ollinger, O. (1980). Measurement of the oxygen cycle: The mass spectrometric analysis of gases dissolved in a liquid phase. *Methods in Enzymology*, *69*, 547–560. https://doi.org/10.1016/S0076-6879(80)69054-5

Raven, J. A. (2013). Iron acquisition and allocation in stramenopile algae. *Journal of Experimental Botany*, *64*(8), 2119–2127. https://doi.org/10.1093/jxb/ert121

Renger, G. (2011). Light induced oxidative water splitting in photosynthesis: Energetics, kinetics and mechanism. *Journal of Photochemistry and Photobiology B: Biology*, *104*(1), 35–43. https://doi.org/10.1016/j.jphotobiol.2011.01.023

Sarmiento, J. L., & Bender, M. (1994). Carbon biogeochemistry and climate change. *Photosynthesis Research*, *39*(3), 209–234. https://doi.org/10.1007/BF00014585

Sarmiento, J. L., Hughes, T. M. C., Stouffer, R. J., & Manabe, S. (1998). Simulated response of the ocean carbon cycle to anthropogenic climate warming. *Nature*, *393*(6682), 245–249. https://doi.org/10.1038/30455

Seppey, M., Manni, M., & Zdobnov, E. M. (2019). BUSCO: Assessing Genome Assembly and Annotation Completeness. In M. Kollmar (Ed.), *Gene Prediction: Methods and Protocols* (pp. 227–245). Springer. https://doi.org/10.1007/978-1-4939-9173-0_14

Shaked, Y., Kustka, A. B., & Morel, F. M. M. (2005). A general kinetic model for iron acquisition by eukaryotic phytoplankton. *Limnology and Oceanography*, *50*(3), 872–882. https://doi.org/10.4319/lo.2005.50.3.0872

Shen, C., & Hopkinson, B. M. (2015). Size scaling of extracellular carbonic anhydrase activity in centric marine diatoms. *Journal of Phycology*, *51*(2), 255–263. https://doi.org/10.1111/jpy.12269

Shikanai, T. (2007). Cyclic Electron Transport Around Photosystem I: Genetic Approaches. *Annual Review of Plant Biology*, *58*(1), 199–217. https://doi.org/10.1146/annurev.arplant.58.091406.110525

Smetacek, V., Klaas, C., Strass, V. H., Assmy, P., Montresor, M., Cisewski, B., Savoye, N., Webb, A., d'Ovidio, F., Arrieta, J. M., Bathmann, U., Bellerby, R., Berg, G. M., Croot, P., Gonzalez, S., Henjes, J., Herndl, G. J., Hoffmann, L. J., Leach, H., … Wolf-Gladrow, D. (2012). Deep carbon export from a Southern Ocean iron-fertilized diatom bloom. *Nature*, *487*(7407), 313–319. https://doi.org/10.1038/nature11229

Spudich, J. L. (2006). The multitalented microbial sensory rhodopsins. *Trends in Microbiology*, *14*(11), 480–487. https://doi.org/10.1016/j.tim.2006.09.005

Spudich, J. L., Yang, C.-S., Jung, K.-H., & Spudich, E. N. (2000). Retinylidene Proteins: Structures and Functions from Archaea to Humans. *Annual Review of Cell and Developmental Biology*, *16*(1), 365–392. https://doi.org/10.1146/annurev.cellbio.16.1.365

Stoeckenius, W., & Bogomolni, R. A. (1982). Bacteriorhodopsin and Related Pigments of Halobacteria. *Annual Review of Biochemistry*, *51*(1), 587–616. https://doi.org/10.1146/annurev.bi.51.070182.003103

Strzepek, R. F., Maldonado, M. T., Hunter, K. A., Frew, R. D., & Boyd, P. W. (2011). Adaptive strategies by Southern Ocean phytoplankton to lessen iron limitation: Uptake of organically complexed iron and reduced cellular iron requirements. *Limnology and Oceanography*, *56*(6), 1983–2002. https://doi.org/10.4319/lo.2011.56.6.1983

Sunda, W. G., & Huntsman, S. A. (1995). Iron uptake and growth limitation in oceanic and coastal phytoplankton. *Marine Chemistry*, *50*(1–4), 189–206. https://doi.org/10.1016/0304-4203(95)00035-P

Sunda, W. G., & Huntsman, S. A. (1997). Interrelated influence of iron, light and cell size on marine phytoplankton growth. *Nature*, *390*(6658), 389–392. https://doi.org/10.1038/37093

Sunda, W., Price, N. M., & Morel, F. M. M. (2005). *Algal Culturing Techniques*. Elsevier.

Tang, S., Lomsadze, A., & Borodovsky, M. (2015). Identification of protein coding regions in RNA transcripts. *Nucleic Acids Research*, *43*(12), e78–e78. https://doi.org/10.1093/nar/gkv227

Timmermans, K. R., & Wagt, B. V. D. (2010). Variability in Cell Size, Nutrient Depletion, and Growth Rates of the Southern Ocean Diatom Fragilariopsis Kerguelensis (bacillariophyceae) After Prolonged Iron Limitation1. *Journal of Phycology*, *46*(3), 497–506. https://doi.org/10.1111/j.1529-8817.2010.00827.x

Torre, J. R. de la, Christianson, L. M., Béjà, O., Suzuki, M. T., Karl, D. M., Heidelberg, J., & DeLong, E. F. (2003). Proteorhodopsin genes are distributed among divergent marine bacterial taxa. *Proceedings of the National Academy of Sciences*, *100*(22), 12830–12835. https://doi.org/10.1073/pnas.2133554100

Vader, A., Laughinghouse, H. D., Griffiths, C., Jakobsen, K. S., & Gabrielsen, T. M. (2018). Proton-pumping rhodopsins are abundantly expressed by microbial eukaryotes in a high-Arctic fjord. *Environmental Microbiology*, *20*(2), 890–902. https://doi.org/10.1111/1462-2920.14035

Watson, A. J., Bakker, D. C. E., Ridgwell, A. J., Boyd, P. W., & Law, C. S. (2000). Effect of iron supply on Southern Ocean CO 2 uptake and implications for glacial atmospheric CO 2. *Nature*, *407*(6805), 730–733. https://doi.org/10.1038/35037561

Zybailov, B., Mosley, A. L., Sardiu, M. E., Coleman, M. K., Florens, L., & Washburn, M. P. (2006). Statistical Analysis of Membrane Proteome Expression Changes in Saccharomyces cerevisiae. *Journal of Proteome Research*, *5*(9), 2339–2347. https://doi.org/10.1021/pr060161n